

**EXPERIMENTAL STUDY ON THE IN-PLANE  
BEHAVIOR OF STANDING SEAM ROOF ASSEMBLY  
AND ITS USE IN LATERAL BRACING OF RAFTERS**

Gengrui Wei, Benjamin W. Schafer, Michael Seek, Matthew R. Eatherton

January 2020

COLD-FORMED STEEL RESEARCH CONSORTIUM  
REPORT SERIES  
**CFSRC R-2020-02**

#### About the authors

G. Wei is a Ph.D. candidate at Virginia Tech working with advisor M.R. Eatherton, Associate Professor at Virginia Tech. Professor B.W. Schafer of Johns Hopkins University and Associate Professor M. Seek of Old Dominion University provided oversight and guidance on this project.

#### CFSRC Information

The Cold-Formed Steel Research Consortium (CFSRC) is a multi-institute consortium of university researchers dedicated to providing world-leading research that enables structural engineers and manufacturers to realize the full potential of structures utilizing cold-formed steel. More information can be found at [www.cfsrc.org](http://www.cfsrc.org). All CFSRC reports are hosted permanently by the Johns Hopkins University library in the DSpace collection: <https://jscholarship.library.jhu.edu/handle/1774.2/40427>.

#### SDII Information

The Steel Diaphragm Innovation Initiative (SDII) is a multi-year industry-academic partnership to advance the seismic performance of steel floor and roof diaphragms utilized in steel buildings through better understanding of diaphragm-structure interaction, new design approaches, and new three-dimensional modeling tools that provided enhanced capabilities to designers utilizing steel diaphragms in their building systems. SDII was created through collaboration between the American Iron and Steel Institute and the American Institute of Steel Construction with contributions from the Steel Deck Institute, the Metal Building Manufacturers Association, and the Steel Joist Institute in partnership with the Cold-Formed Steel Research Consortium; including, researchers from Johns Hopkins University, Virginia Tech, Northeastern University, and Walter P Moore.

#### **Acknowledgements**

This work was supported by the Metal Building Manufacturers Association (MBMA) and is part of the Steel Diaphragm Innovation Initiative which is funded by AISC, AISI, SDI, SJI, and MBMA. Materials were donated by Chief Buildings, Schulte Building Systems, and Bay Insulations Systems. Assistance with the seaming process was provided by Ethan Smith of DI Roof Seamers. The authors also would like to thank Mr. Mahyar Zarat-Basir and Mr. Carl Miller for their help with preparing and conducting the tests. Any opinions expressed in this paper are those of the authors alone, and do not necessarily reflect the views of the sponsors.

## ABSTRACT

The standing seam roof (SSR) system is the most commonly used roof system for metal buildings due to its superior durability, water tightness, and energy efficiency. In this type of system, SSR panels attach to Z-shaped or C-shaped purlins with clips, and the purlins are in turn connected to rafters (i.e. roof beams). For the design of the rafters against lateral torsional buckling, bottom flange braces provide torsional bracing to the rafter and the SSR system provides some lateral bracing. However, the degree to which the SSR system can restrain the rafter against lateral movement has not previously been studied. The objective of this study is to quantify the in-plane strength and stiffness of the SSR system and identify how this can be used to provide lateral bracing to the rafter.

A total of 11 full-scale standing seam roof specimens were tested to investigate the effects of different standing seam roof configurations (SSR panel type, clip type, thermal insulation, and purlin spacing) on the in-plane stiffness and strength of the SSR system. The resulting stiffness and peak strength of the specimens were tabulated and compared for different SSR configurations.

Results showed that the in-plane load-deformation behavior of SSR systems was governed by clip deformations and that variations in the type of SSR panel or clip can have a major impact on the strength and stiffness of the specimens. A specimen with vertical rib panels was shown to have 16 times more stiffness than a similar specimen with trapezoidal rib panels because the vertical ribs restrain the clip deformation. However, even a small standoff was found to reduce the stiffness of vertical rib SSR assemblies with more than three-fold drop in stiffness as the standoff was increased from 0 in. to 0.4 in. Trapezoidal rib SSR assemblies had consistent strength stiffness with fixed clips having standoff of 0 in. or 0.5 in., but with floating clips the stiffness decreased with increasing standoff. Addition of blanket insulation and thermal blocks were found to result in 60% to 350% increase in stiffness.

A method for using these experimental results in calculations of required bracing for metal building rafters is described. An example is also provided which demonstrates that the SSR roof can contribute to bracing of the rafter and may reduce spacing or size of discrete/point torsional braces.

# TABLE OF CONTENTS

<b>ABSTRACT .....</b>	<b>i</b>
<b>TABLE OF CONTENTS .....</b>	<b>ii</b>
<b>LIST OF TABLES .....</b>	<b>iv</b>
<b>LIST OF FIGURES .....</b>	<b>v</b>
<b>1. INTRODUCTION .....</b>	<b>1</b>
1.1 Overview .....	1
1.2 Motivation .....	2
1.3 Scope of Work .....	4
<b>2. TESTING PROGRAM .....</b>	<b>5</b>
2.1 Test Matrix .....	5
2.2 Specimen Construction .....	8
2.3 Test Setup .....	10
2.4 Instrumentation .....	11
2.5 Loading Protocol .....	12
<b>3. RESULTS AND DISCUSSION .....</b>	<b>14</b>
3.1 Test Results .....	14
3.2 Effect of Different Parameters .....	27
3.2.1 Panel Type .....	27
3.2.2 Clip Type .....	29
3.2.3 Thermal Insulation .....	30
3.2.4 Purlin Spacing .....	31

<b>4. APPLICATION IN DESIGN AND PRACTICE .....</b>	<b>32</b>
4.1 Concepts.....	32
4.2 Example.....	39
4.3 Discussion.....	43
<b>5. CONCLUSIONS AND RECOMMENDATIONS .....</b>	<b>44</b>
5.1 Conclusions.....	44
5.2 Recommendations for Future Work .....	45
<b>REFERENCES.....</b>	<b>47</b>
<b>APPENDIX.....</b>	<b>48</b>

## LIST OF TABLES

Table 1 SSR Test Matrix.....	6
Table 2 Measured Seam Width.....	9
Table 3 Displacement of Middle Purlin When Clips Failed and Load at First Clip Failure .....	20
Table 4 Maximum Load and Secant Stiffness of Specimens.....	27
Table 5 Maximum Load and Secant Stiffness $K_{40\%}$ of Specimens with Different Panel Types .....	28
Table 6 Maximum Load and Secant Stiffness $K_{40\%}$ of Specimens with Different Clip Types .....	29
Table 7 Maximum Load and Secant Stiffness $K_{40\%}$ of Specimens with or without Thermal Insulation .....	30
Table 8 Provided Strength and Stiffness per Clip of SSR for Lateral Bracing of Rafter.....	36

## LIST OF FIGURES

Figure 1 Schematic view of an SSR system .....	1
Figure 2 Lateral bracing and load transfer of main frame.....	3
Figure 3 Lateral load from rafter lateral torsional buckling acting on purlins and SSR panels .....	4
Figure 4 Typical specimen layout.....	6
Figure 5 SSR panels used in the experimental program.....	7
Figure 6 Clips used in the experimental program.....	7
Figure 7 Specimen construction process .....	8
Figure 8 Pictures showing the seaming process in sequential order .....	9
Figure 9 Schematic view of test setup .....	10
Figure 10 Details of fixed support.....	11
Figure 11 Details of sliding support .....	11
Figure 12 Reaction Frame .....	11
Figure 13 Schematic view of instrumentation layout.....	12
Figure 14 Picture of test setup and specimen prior to testing.....	13
Figure 15 Typical deformed shape of clip bending and panel buckling (from Specimen 7) .....	15
Figure 16 Mechanical detachment of clips from top (left) and bottom (right) (from Specimen 8) .....	15
Figure 17 Tearing of clip material at the bottom (from Specimen 7).....	15
Figure 18 Load-displacement curve of Specimen 1.....	16
Figure 19 Load-displacement curve of Specimen 2.....	16
Figure 20 Load-displacement curve of Specimen 3.....	17
Figure 21 Load-displacement curve of Specimen 4.....	17
Figure 22 Load-displacement curve of Specimen 5.....	17
Figure 23 Load-displacement curve of Specimen 6.....	18
Figure 24 Load-displacement curve of Specimen 7.....	18
Figure 25 Load-displacement curve of Specimen 8.....	18
Figure 26 Load-displacement curve of Specimen 9.....	19
Figure 27 Load-displacement curve of Specimen 10.....	19

Figure 28 Load-displacement curve of Specimen 11 .....	19
Figure 29 Example displacement curves for all purlins (from Specimen 1) .....	21
Figure 30 Free body diagram of clips and panels .....	21
Figure 31 Middle purlin clip and panel deformation curves .....	24
Figure 32 Panel slip measurement affected by panel buckling (from Specimen 2) .....	26
Figure 33 Slip between adjacent panels (left: Specimen 4; right: Specimen 5) .....	26
Figure 34 Stiffening and restraint of clips by standing seams with different profiles.....	28
Figure 35 Load-displacement curves of specimens with different panel types .....	28
Figure 36 Load-displacement curves of specimens with different clip types .....	30
Figure 37 Load-displacement curves of specimens with or without thermal insulation .....	31
Figure 38 Load-displacement curves of specimens with different purlin spacing .....	31
Figure 39 Plan view of typical metal building roof framing with assumed buckled shape of rafter .....	32
Figure 40 Section view of adjacent rafters braced by SSR and flange braces with assumed buckled shape .....	32
Figure 41 Structure assemblage for analyzing torsional bracing strength and stiffness of rafter provided by flange brace and purlin.....	37
Figure 42 Moment and axial force diagram of the assemblage subjected to concentrated moment applied at the top of rafter .....	37
Figure 43 Plan view of roof framing detail of prototype metal building.....	40
Figure A1-1 Load-displacement curve for Specimen 1 .....	48
Figure A1-2 Purlin displacements of Specimen 1 .....	48
Figure A1-3 Deformed shape of Specimen 1 .....	49
Figure A1-4 Clip damage of Specimen 1 .....	49
Figure A2-1 Load-displacement curve for Specimen 2 .....	49
Figure A2-2 Purlin displacements of Specimen 2 .....	50
Figure A2-3 Deformed shape of Specimen 2 .....	50
Figure A2-4 Clip damage of Specimen 2 .....	50
Figure A3-1 Load-displacement curve for Specimen 3 .....	51

Figure A3-2 Purlin displacements of Specimen 3 .....	51
Figure A3-3 Deformed shape of Specimen 3 .....	51
Figure A3-4 Clip damage of Specimen 3 .....	52
Figure A4-1 Load-displacement curve for Specimen 4 .....	52
Figure A4-2 Purlin displacements of Specimen 4 .....	52
Figure A4-3 Deformed shape of Specimen 4 .....	53
Figure A4-4 Clip damage of Specimen 4 .....	53
Figure A5-1 Load-displacement curve for Specimen 5 .....	53
Figure A5-2 Purlin displacements of Specimen 5 .....	54
Figure A5-3 Deformed shape of Specimen 5 .....	54
Figure A5-4 Clip damage of Specimen 5 .....	54
Figure A6-1 Load-displacement curve for Specimen 6 .....	55
Figure A6-2 Purlin displacements of Specimen 2 .....	55
Figure A6-3 Deformed shape of Specimen 6 .....	55
Figure A6-4 Clip damage of Specimen 6 .....	56
Figure A7-1 Load-displacement curve for Specimen 7 .....	56
Figure A7-2 Purlin displacements of Specimen 7 .....	56
Figure A7-3 Deformed shape of Specimen 7 .....	57
Figure A7-4 Clip damage of Specimen 7 .....	57
Figure A8-1 Load-displacement curve for Specimen 8 .....	57
Figure A8-2 Purlin displacements of Specimen 8 .....	58
Figure A8-3 Deformed shape of Specimen 8 .....	58
Figure A8-4 Clip damage of Specimen 8 .....	58
Figure A9-1 Load-displacement curve for Specimen 9 .....	59
Figure A9-2 Purlin displacements of Specimen 9 .....	59
Figure A9-3 Deformed shape of Specimen 9 .....	59
Figure A9-4 Clip damage of Specimen 9 .....	60
Figure A10-1 Load-displacement curve for Specimen 10 .....	60
Figure A10-2 Purlin displacements of Specimen 10 .....	60

Figure A10-3 Deformed shape of Specimen 10 .....	61
Figure A10-4 Clip damage of Specimen 10 .....	61
Figure A11-1 Load-displacement curve for Specimen 11 .....	61
Figure A11-2 Purlin displacements of Specimen 11 .....	62
Figure A11-3 Deformed shape of Specimen 11 .....	62
Figure A11-4 Clip damage of Specimen 11 .....	62

# 1. INTRODUCTION

## 1.1 Overview

Metal building systems are popular for low-rise buildings because of their fast construction and cost efficiency. One of the main components of a metal building is the roof system, a common type of which is the standing seam roof (SSR) system. An SSR system consists of purlins, clip fasteners, SSR panels, and optional thermal blocks and blanket insulation, as is shown in Figure 1. Z-shaped or C-shaped purlins provide support for the roof and are attached to the frames of the building. The SSR panels are light-gauge corrugated metal sheets which span between the purlins and connect to each other through the standing seam created by roll forming the vertical or trapezoidal legs along the panel edges. Clip fasteners are installed on the purlins and extend up into the standing seam, which after the seam is crimped provides a connection between the roof panels and purlins. Depending on the need for thermal insulation, thermal blocks and blanket insulation can also be installed underneath the roof panels.

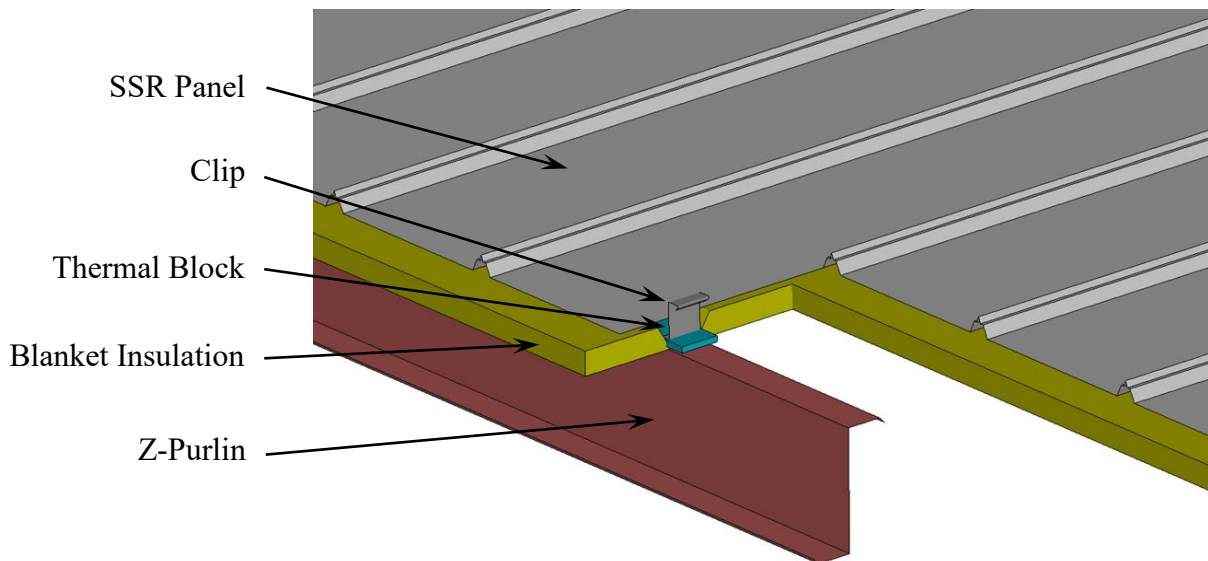


Figure 1 Schematic view of an SSR system

The SSR system is widely used in metal buildings due to several advantages over some conventional through-fastened metal deck roof systems. It eliminates the need to create holes

in the roof panels for deck attachment (e.g. welds, power actuated fasteners, or screws through metal roof deck typical in steel-framed buildings), and as a result can improve water tightness of the roof system and prolong its life cycle. The clip fasteners are hidden in the standing seams and are not exposed to outside environmental conditions which protects them against accelerated corrosion and failure. This feature also reduces the cost of regular maintenance. In addition, the SSR system has superior performance when subjected to thermal variations. The flexibility of the clip fasteners and the standing seam allow the thermal expansion and contraction of the roof panels in both transverse and longitudinal directions. The reflection of sun's ray by the metal roof decreases the heat transfer and improves the energy efficiency of the cooling system, while optional thermal blocks and blanket insulation provide further energy efficiency. The favorable architectural appearance of the SSR system is also one of the reasons why it has become the first choice for many buildings.

Despite multiple advantages of the SSR system, it also presents some challenges. It's usually considered more expensive than some other alternatives, partially due to its labor-intensive installation process including the spacing and fastening of clips on the purlins, aligning and snapping the legs of roof panels next to each other, and roll forming (i.e. crimping) the standing seam with tools and machines. Also, the standing seam roof provides only limited stiffness or strength as a diaphragm because clips and seams allow movement.

## **1.2 Motivation**

There are different types of bracing at the roof level that restrain lateral movement of the entire building and restrain lateral movement of individual members. The in-plane bracing in the roof plane of a metal building is provided by tension rod or cable bracing with X braces attached to the web of the rafter near the top flange. Another type of bracing involves top and bottom flange bracing of the rafter to prevent lateral torsional buckling of the rafter. This type of bracing is typically provided by the purlins at the top flange and diagonal flange braces that extend from the purlin to the bottom flange.

The flange brace and purlin create frame action that acts as torsional bracing for the rafter. Additionally, the SSR system provides some restraint against rafter lateral motion because it resists relative longitudinal motion of purlins. That is, for purlins not located at the point where roof X braces intersect the rafter, the SSR system restrains longitudinal motion of the purlin relative to adjacent purlins. This concept is demonstrated in Figure 2 as the lateral force associated with rafter lateral torsional buckling is applied to the purlins. A simplified free-body diagram of the SSR system with lateral bracing load is shown in Figure 3. It is noted that this loading configuration is highly idealized as a single bracing load and simple supports. In the context of AISC 360-16 (AISC 2016), the locations where the roof X braces connect to the rafter may be considered point bracing for global stability, while the SSR system provides point bracing at the interior purlin locations for local instability. Also, there may be loads imposed at more than one lateral brace, and these loads may not be going the same direction.

AISC 360-16 (AISC 2016) Appendix 6 provides equations for calculating the required stiffness and strength for beam point bracing. However, the in-plane resistance of the SSR panels and their ability to brace the rafter have not been previously studied. It is therefore necessary to conduct experimental tests to investigate the in-plane bending stiffness and strength of SSR assemblies.

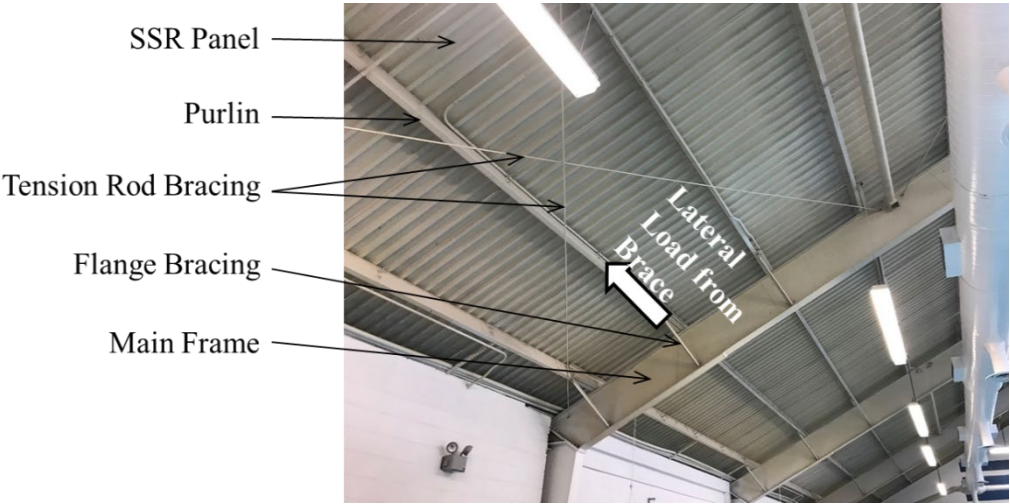


Figure 2 Lateral bracing and load transfer of main frame

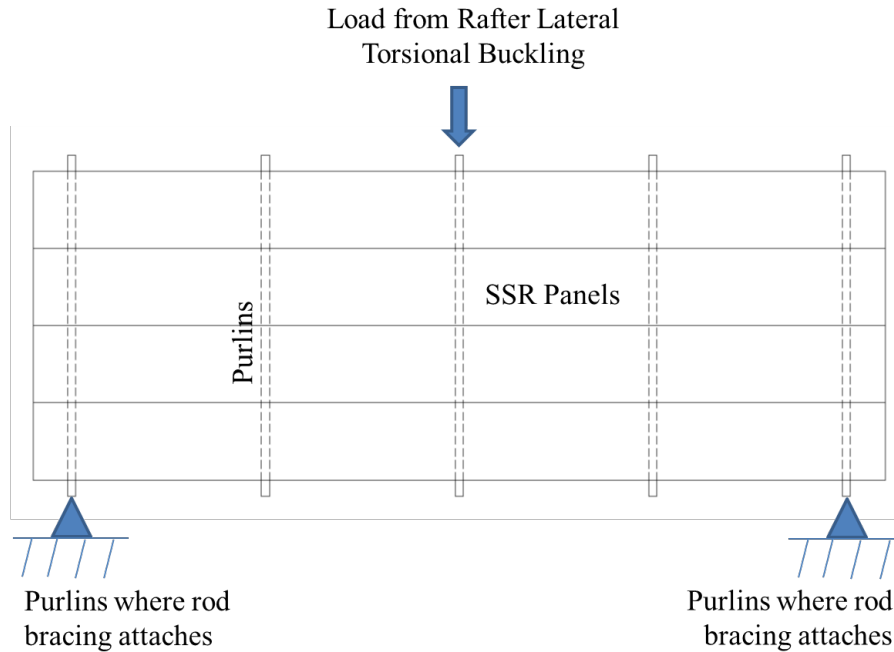


Figure 3 Lateral load from rafter lateral torsional buckling acting on purlins and SSR panels

### 1.3 Scope of Work

Eleven full-scale in-plane bending tests on SSR systems were conducted at the Thomas M. Murray Structures Lab of Virginia Tech. Each specimen was a 22 ft long SSR unit with panels and purlins that represent the portion of a roof between points where roof X bracing attaches to the rafter. The objective of this study is to investigate the in-plane strength and stiffness of the SSR system for restraining the purlins against longitudinal movement. Each specimen had a unique configuration to study the effect of different parameters including SSR panel profiles, SSR panel width, type of clip and screw fasteners, clip standoff, and use of thermal blocks and blanket insulation. Results from the tests were analyzed and compared to the bracing requirements in AISC 360-16 for an example rafter.

## 2. TESTING PROGRAM

### 2.1 Test Matrix

There were 11 specimens with different configurations as given in Table 1 and typical specimen layout shown in Figure 4. The specimens had 4 SSR panels and 5 or 9 purlins depending on the purlin spacing. The length of the panels was 22 ft, and the length of the purlins was either 6.5 ft for the specimens with 16 in. wide panels or 9 ft for the specimens with 24 in. wide panels. The parameters considered in developing the test matrix include the following:

- 1) Panel profile. The profiles of the SSR panels are categorized into two main types: trapezoidal rib profile which has sloped legs adjacent to the seam, and vertical rib profile which has vertical legs adjacent to the seam. The different panel profiles are shown in Figure 5.
- 2) Manufacturer. Material for constructing the specimens, including SSR panels, purlins, clips and screw fasteners, were provided by different manufacturers which are referred to as TS-324, MSC, VS-216, and MVP.
- 3) Panel gauge. All the specimens used SSR panels with 24-gauge thickness.
- 4) Panel width. The panels were either 24 in. or 16 in. wide.
- 5) Clip type. Fixed clips are snapped to the male leg of panels and mounted onto the purlin flange. They do not have a slider and are fixed in place. Floating clips are two-piece clips with the body of clip snapped and seamed to the legs of panels, the base installed to the purlin flange, and these two pieces being connected by a mechanism to allow sliding of the main body as a unit. Sliding tab clips have a rigid main body with a sliding tab that fits into the seam and slides along a slotted hole on the main body. Figure 6 shows the different clips used to construct the specimens.
- 6) Clip standoff. To allow for insulation to be sandwiched between the purlin and the panels, the height of the clip may be extended to increase the distance between the top of the purlin and the underside of panels. This distance is referred to as standoff and was varied in the tests from 0 to 1.5 in.
- 7) Insulation. Two specimens were constructed with blanket insulation, one of which also included thermal blocks.

8) Purlin spacing. Only one specimen used purlins spaced at 2.5 ft and the rest all had a typical purlin spacing of 5 ft.

Table 1 SSR Test Matrix

Specimen	Panel Profile	Manufacturer	Panel Gauge	Panel Width (in.)	Clip Type	Standoff (in)	Insulation	Purlin Spacing (ft)
1	Trapezoidal	TS-324	24	24	Fixed	0	No	5
2	Trapezoidal	TS-324	24	24	Floating	0.5	No	5
3	Trapezoidal	MSC	24	24	Sliding tab	0.4	No	5
4	Vertical	VS-216	24	16	Fixed	0	No	5
5	Vertical	VS-216	24	16	Floating	3/8	No	5
6	Vertical	MVP	24	16	Floating	0.4	No	5
7	Trapezoidal	TS-324	24	24	High Fixed	0.5	No	5
8	Trapezoidal	TS-324	24	24	High Floating	1.5	No	5
9	Trapezoidal	TS-324	24	24	High Floating	1.5	9 in. insulation 1 in. thermal block	5
10	Trapezoidal	MSC	24	24	Sliding tab	0.4	6 in. insulation no thermal block	5
11	Trapezoidal	TS-324	24	24	Fixed	0	No	2.5

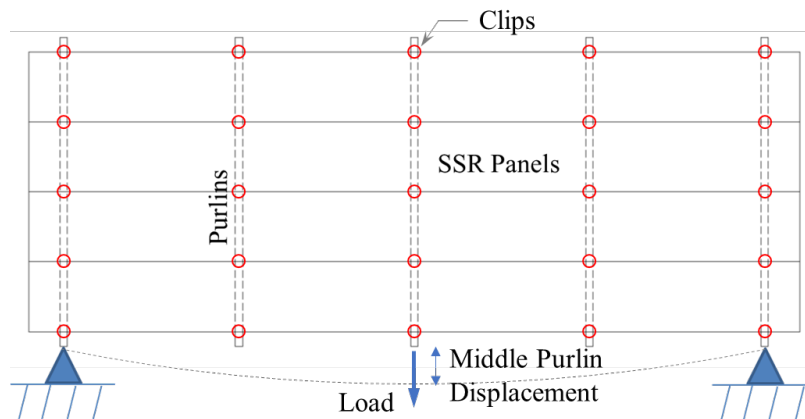


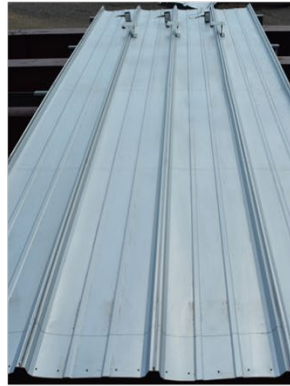
Figure 4 Typical specimen layout

SS2-4A5CD5F4-  
24GA TS-324 Panel  
Galv- Clear Acrylic



Specimens 1, 2, 7, 8, 9, 11

MSC (trapezoidal)-  
24"- Roof Panel



Specimens 3, 10

SS14A5A7975--24  
GA VS-216 Panel  
Galv-Acrylic Coated



Specimens 4, 5

MVP (vertical) panel-  
16" CT1188919RV264



Specimen 6

Figure 5 SSR panels used in the experimental program

Fixed - FC461 0  
standoff



Specimens 1, 11  
(with TS-324)

Floating - MPS 602  
0.5" standoff



Specimen 2  
(with TS-324)

Sliding tab - STC  
0.5" standoff



Specimens 3, 10  
(with MSC)

Fixed - FC10200  
0 standoff



Specimen 4  
(with VS-216)

Floating - MC 1203  
3/8" standoff



Specimen 5  
(with VS-216)

Floating - MVP short clip  
0.4" standoff



Specimen 6  
(with MVP)

Fixed - FC462  
0.5" standoff



Specimen 7  
(with TS-324)

High Floating - MPS 603  
1.5" standoff



Specimens 8, 9  
(with TS-324)

Figure 6 Clips used in the experimental program

## 2.2 Specimen Construction

Figure 7 shows the process of constructing the specimens. Two C-channels with a length of 22 ft were temporarily used to space and position the purlins, which were mounted at the bottom flange of both ends to the channels with self-drilling screws (Figure 7a). Thermal blocks and blanket insulation (if any) were placed on the purlins (Figure 7e). Clips were then installed onto the top flange with self-tapping screws starting from one end of each purlin (Figure 7b). The SSR panels were aligned such that the leg of the panel could be attached to the clips (Figure 7c). Once the previous panel was in place, clips were fastened on the other edge of the panel and this process was repeated until all the panels and clips were installed (Figures 7d, 7f).

A final step of construction before testing each of these specimens was to seam the panels as shown in Figure 8. A professional roof seamer assisted with the seaming process. A hand seamer was used to create a starting seam at one end (Figures 8a, 8b) followed by running a self-propelling roll forming machine to seam the entire legs of the adjacent panels (Figures 8c, 8d). Depending on the panel profiles, a single lock (e.g. Specimen 6) or a double lock (e.g. Specimen 4) standing seam was made. Table 2 shows the average and standard deviation of seam width measured with a digital caliper at six arbitrary locations (on clip or off clip) of each specimen.



Figure 7 Specimen construction process



Figure 8 Pictures showing the seaming process in sequential order

Table 2 Measured Seam Width

Specimen	On clip		Off clip	
	avg (in.)	std (in.)	avg (in.)	std (in.)
1	0.500	0.007	0.459	0.006
2	0.484	0.002	0.444	0.002
3	0.370	0.014	0.321	0.004
4	0.471	0.009	0.454	0.004
5	0.478	0.007	0.451	0.005
6	0.304	0.012	0.338	0.005
7	0.501	0.017	0.488	0.016
8	0.506	0.017	0.492	0.024
9	0.498	0.030	0.491	0.018
10	0.370	0.012	0.323	0.005
11	0.498	0.018	0.447	0.023

## 2.3 Test Setup

A reaction frame was built to test the SSR specimens as shown in Figure 9. It consisted of five 36-inch tall built-up beams spaced at 5 ft with two 12-inch tall built up beams attached to the top flanges at both ends. Fixed supports for the exterior purlins were made with angles (see Figure 10) that were bolted to the reaction beams and the purlins to simulate the point bracing location (i.e. hard point) at the ends of the roof X bracing. For interior purlins, angle supports with slots to facilitate the sliding of purlins were attached to the interior reaction beams (see Figure 11). A hydraulic jack with a capacity of 25 kips was connected to the web of the reaction beam and the other end of the jack was attached to a load cell and then two 60 in. x 6 in. x ¼ in. plates which were used to sandwich and bolt to the web of the middle purlin. The orientation of the clips was kept consistent for all the specimens with the base of the clips facing the hydraulic jack. A view of the reaction frame is also shown in Figure 12.

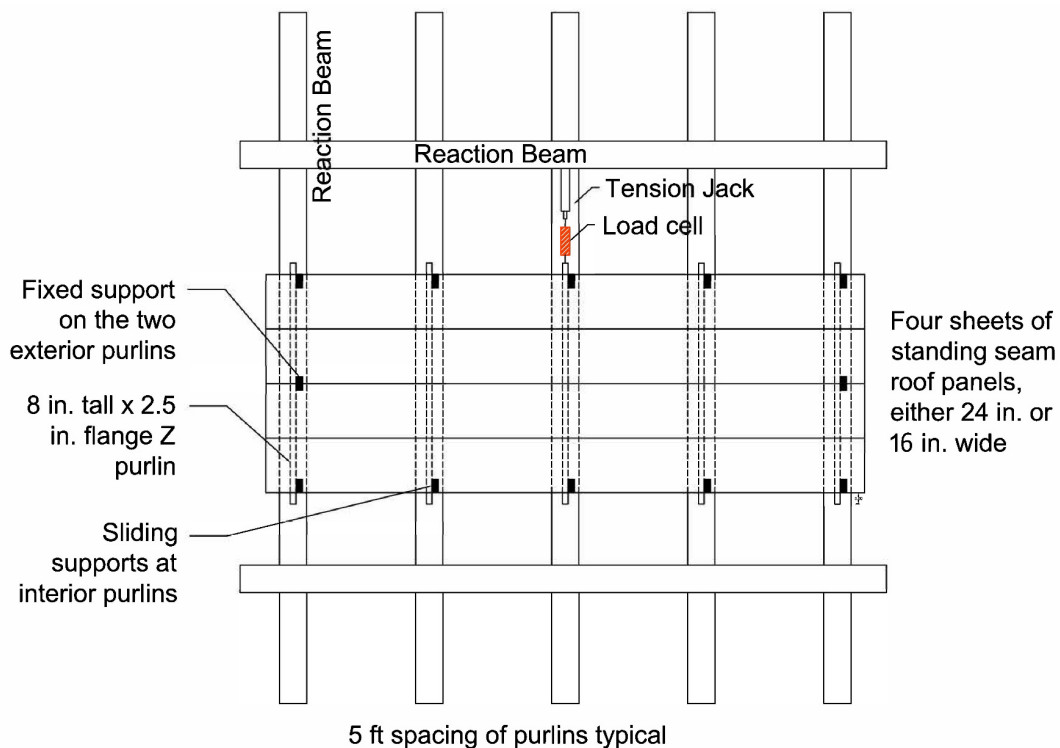


Figure 9 Schematic view of test setup

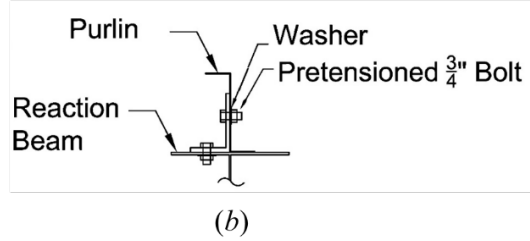
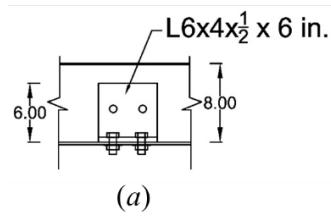


Figure 10 Details of fixed support

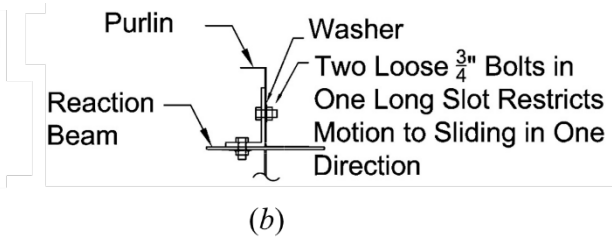
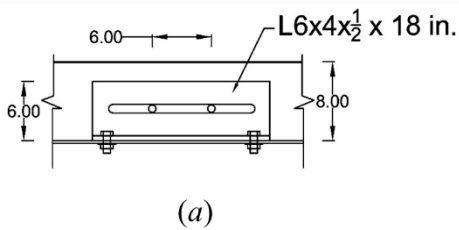


Figure 11 Details of sliding support



Figure 12 Reaction Frame

## 2.4 Instrumentation

A total of ten string potentiometers were used as shown in Figure 13. Five of them (SP01 to SP05) measured the longitudinal displacement of each purlin relative to the ground. Two string potentiometers measured the relative displacement between the middle purlin and the SSR panels (SP09 and SP10). The other three string potentiometers measured the relative slip between adjacent SSR panels (SP06 to SP08). A picture of the complete test setup with instrumentation is shown in Figure 14.

## 2.5 Loading Protocol

A tension load was applied by the hydraulic jack to the north end of the middle purlin. The load was applied incrementally with a hydraulic pump followed with a waiting period of approximately 10 seconds to allow the deformation of the specimens to stabilize. Each test was considered completed if any of the following conditions occurred: 1) the specimen failed with substantial loss of strength (typical); 2) any of the displacement transducers reached the limit of their stroke (e.g. Specimens 2 and 10); 3) the bolt on the middle purlins reached the end of the sliding support (e.g. Specimen 7).

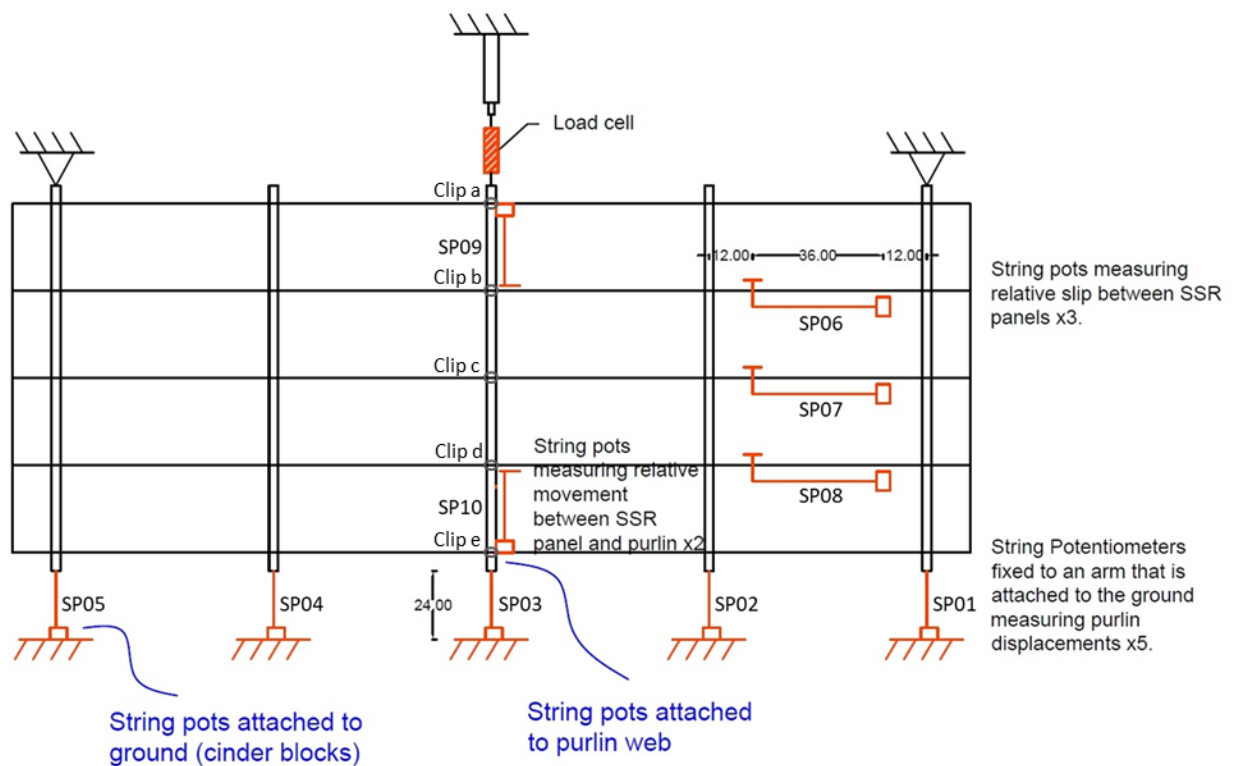


Figure 13 Schematic view of instrumentation layout



Figure 14 Picture of test setup and specimen prior to testing

### 3. RESULTS AND DISCUSSION

Data of applied load and displacements were collected during the tests. Results are presented and discussed in this section. More test results are given in the Appendix.

#### 3.1 Test Results

The load path for the specimen, as supported by the deformed shape of specimens, was: 1) load was applied to the middle purlin, 2) load transferred to the SSR panels through clips on the middle purlin, 3) SSR panels transferred load from the middle to the edges through bending and shear of the panels, 4) load transferred to the exterior purlins through clips, and 5) load transferred from exterior purlins to reaction frame. All specimens exhibited a similar progression of behavior. In the early stage of the load-deformation response, the majority of the deformation resulted from bending of the clips (see Figure 15). After the clips bent such that the clip leg made an acute angle with the SSR panels, the clip tension contributed to the in-plane load resistance and there was an increase in specimen stiffness. This phenomenon was most notable with clips having increased standoff. Panel buckling occurred (Figure 16) with increasing deformation of the clips, resulting in a minor drop of load. As the applied displacement increased, clips could be mechanically detached from the panel seams at the top or bottom depending on the type of clips, or fractured at the bottom due to the bearing of screw fasteners against holes on the base of the clips (as shown in Figures 17 and 18), which caused substantial loss of strength and led to the failure of the specimen.



Figure 15 Typical deformed configuration with clip bending (from Specimen 7)



Figure 16 Typical deformed shape after panel buckling (from Specimen 7)



Figure 17 Mechanical detachment of clips from top (left) and bottom (right) (from Specimen 8)



Figure 18 Tearing of clip material at the bottom (from Specimen 7)

Figures 19 to 29 show the applied load versus middle purlin displacement curve and the progression of failure for each specimen. Clips a, b, c, d, and e refer to the clips attached to the middle purlin in sequential order with Clip a being the one closest to the hydraulic jack (see Figure 13). Displacements of the middle purlin when clips failed are given in Table 3, and the load at

which the first clip failed for each specimen is also provide which can be considered as the lower bound strength of each clip configuration.

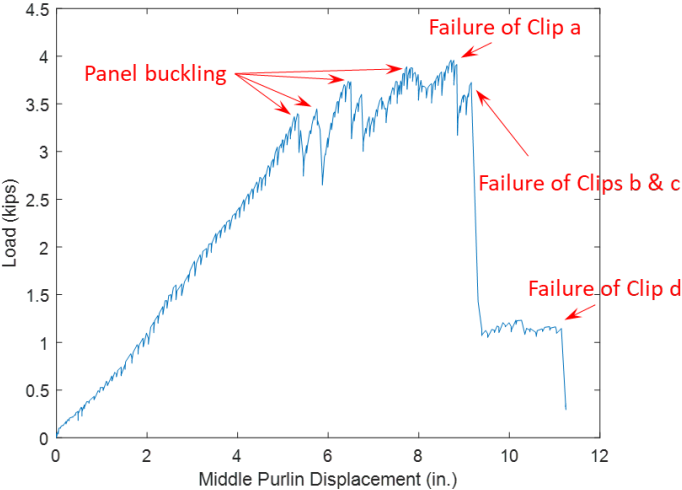


Figure 19 Load-displacement curve of Specimen 1

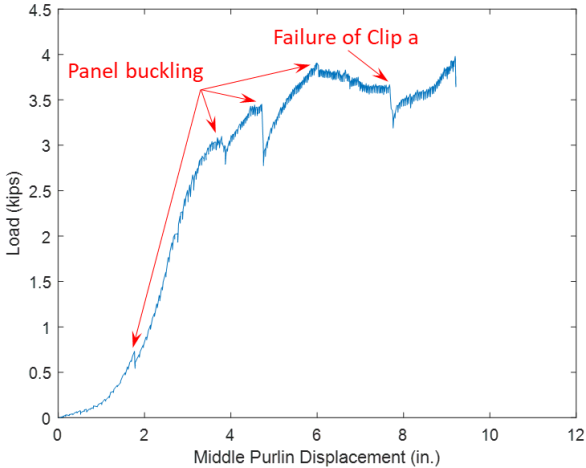


Figure 20 Load-displacement curve of Specimen 2

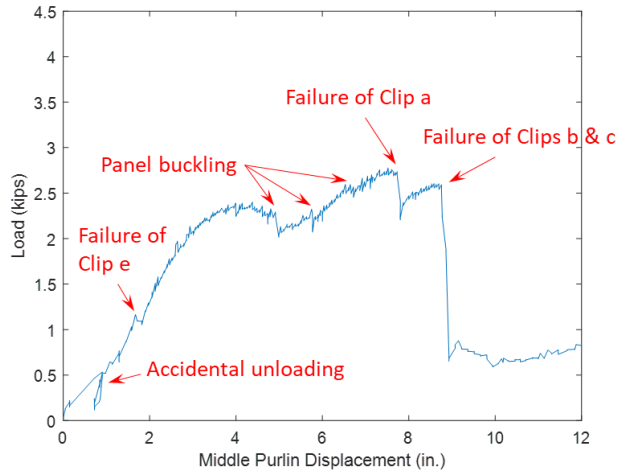


Figure 21 Load-displacement curve of Specimen 3

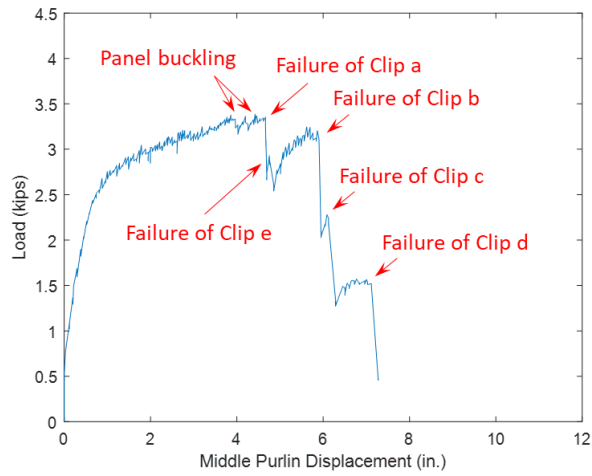


Figure 22 Load-displacement curve of Specimen 4

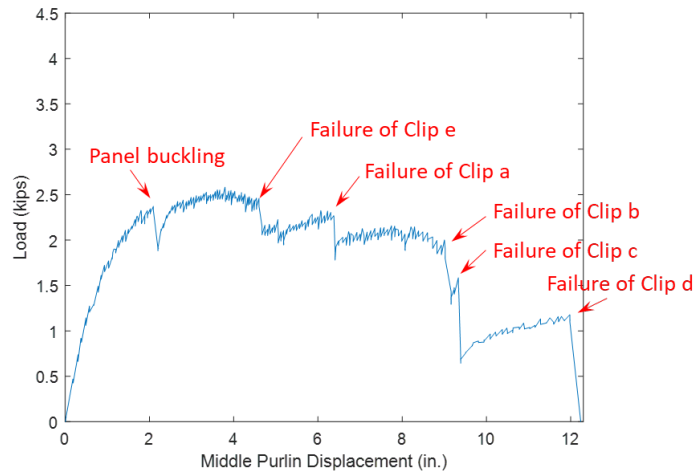


Figure 23 Load-displacement curve of Specimen 5

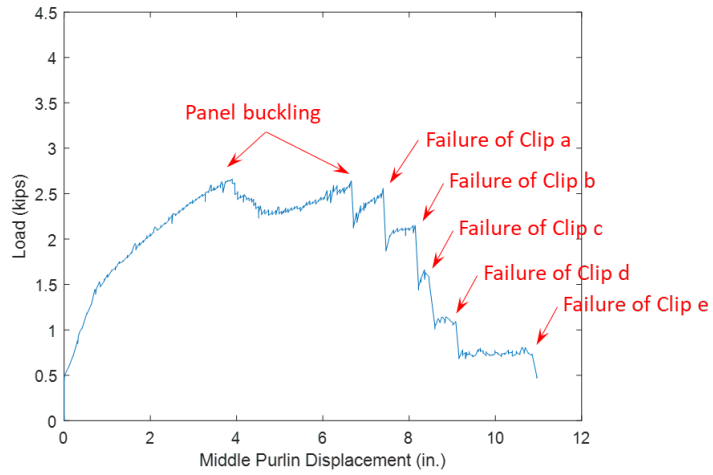


Figure 24 Load-displacement curve of Specimen 6

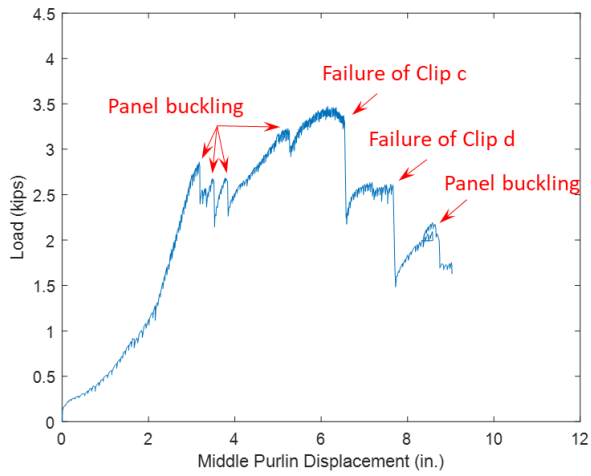


Figure 25 Load-displacement curve of Specimen 7

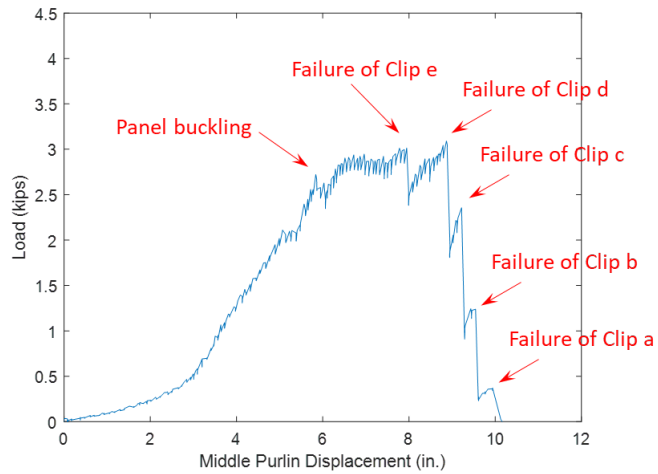


Figure 26 Load-displacement curve of Specimen 8

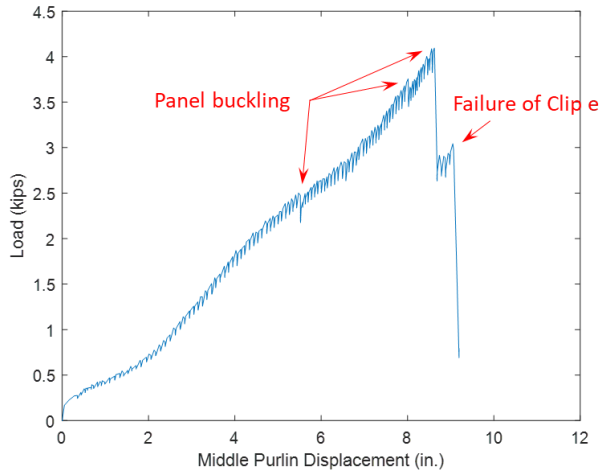


Figure 27 Load-displacement curve of Specimen 9

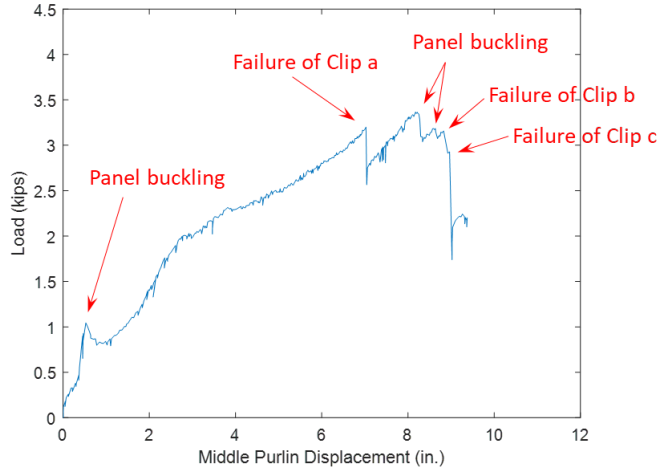


Figure 28 Load-displacement curve of Specimen 10

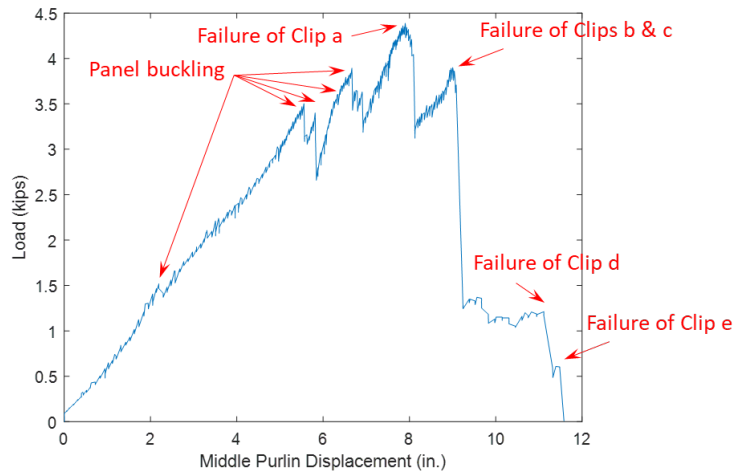


Figure 29 Load-displacement curve of Specimen 11

Table 3 Displacement of Middle Purlin When Clips Failed and Load at First Clip Failure

Specimen	Middle Purlin Displacement at Clip Failure (in)					Load at First Clip Failure (kip)
	Clip a	Clip b	Clip c	Clip d	Clip e	
1	8.84	9.16	9.16	11.15	-	3.96
2	7.69	-	-	-	-	3.63
3	7.73	8.76	8.76	-	1.67	1.17
4	4.67	5.90	6.12	7.12	4.75	3.35
5	6.37	9.00	9.33	11.98	4.60	2.45
6	7.40	8.14	8.46	9.08	10.85	2.56
7	-	-	6.55	7.66	-	3.31
8	9.94	9.54	9.22	8.89	7.95	3.01
9	-	-	-	-	9.05	3.04
10	7.03	8.83	8.97	-	-	3.20
11	8.09	9.08	9.08	11.12	11.48	4.39

- Clip failure did not occur during the test.

Figure 30 shows an example of the displacement curves for all five purlins of Specimen 1 (herein denoted as P1, P2, P3, P4, and P5, corresponding to those which the string potentiometers SP01, SP02, SP03, SP04, and SP05 were attached to, respectively). It can be observed that the exterior purlins P1 and P5 exhibited nearly zero displacement at the fixed supports, while the middle purlin P3 where the load was applied experienced the largest displacement. The two interior purlins P2 and P4 on the sliding supports also moved due to the rigid body movement and in-plane bending of the SSR panels. During the early stages of a typical test, the displacement of P3,  $\delta_3$ , was found to be approximately three times the displacement of P2,  $\delta_2$ , or the displacement of P4,  $\delta_4$ . This is demonstrated by the following calculations where clip deformation dominated the displacements at the beginning of the test while the roof panels moved effectively as a rigid body.

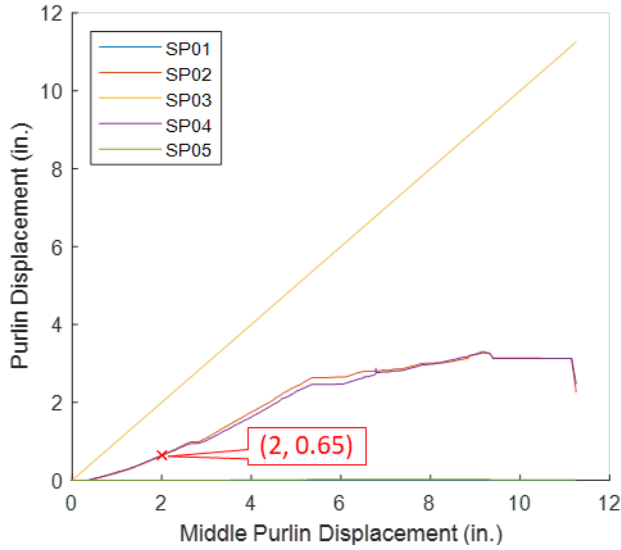


Figure 30 Example displacement curves for all purlins (from Specimen 1)

A free-body diagram of the clips and panels is shown in Figure 31. There are five clips at each purlin, and therefore the stiffness of the clips is shown as  $5k_c$ , where  $k_c$  is the stiffness of one clip. This is a simplifying assumption that all clips contribute equal stiffness even though edge clips may not be as well constrained as interior clips and thus may have lower stiffness in reality.

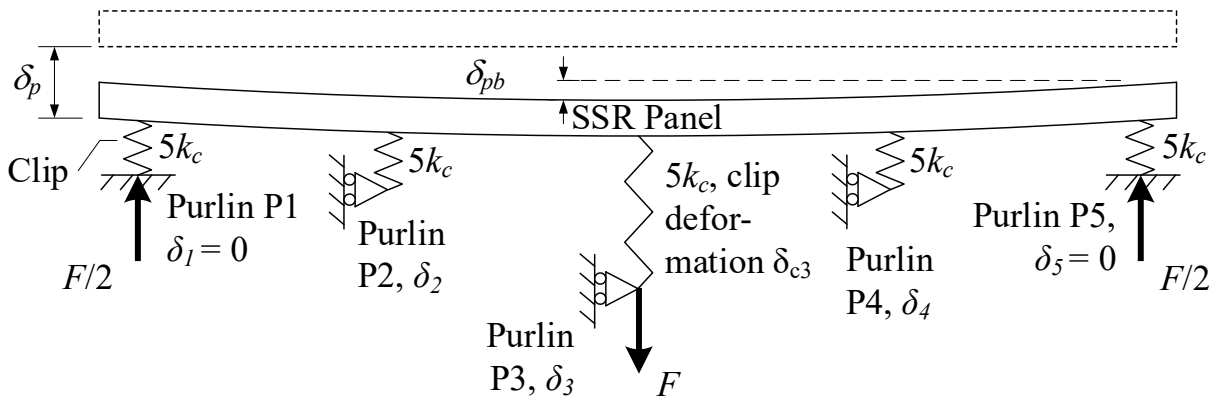


Figure 31 Free body diagram of clips and panels

As the specimen is subjected to a load,  $F$ , at the middle purlin, the corresponding displacement at the middle purlin,  $\delta_3$ , can be calculated as the sum of the clip deformation at purlin P3,  $\delta_{c3}$ , the midspan deformations of the panel,  $\delta_{pb}$ , and the clip deformation at the edge purlins (purlin P1 or P5) which is also equal to the panel rigid body displacement,  $\delta_p$ .

$$\delta_3 = \delta_{c3} + \delta_{pb} + \delta_p \quad (1)$$

The clip deformation on the middle purlin,  $\delta_{c3}$ , is given by:

$$\delta_{c3} = \frac{F}{5k_c} \quad (2)$$

During the early stage of the tests, the SSR panels acted as a rigid body and the deformation of the panels due to in-plane bending was negligible compared to the clip deformation. Hence it is assumed that the panel deformation  $\delta_{pb}$  due to in-plane bending is zero:

$$\delta_{pb} = 0 \quad (3)$$

The rigid body displacement of the panels,  $\delta_p$ , is equal to the deformation of the clips on the exterior purlins at fixed supports and can be obtained by:

$$\delta_p = \frac{F/2}{5k_c} = \frac{F}{10k_c} \quad (4)$$

The displacement of the middle purlin can then be obtained by substituting Eq. (2), Eq. (3), and Eq. (4) into Eq. (1):

$$\delta_3 = \frac{F}{5k_c} + 0 + \frac{F}{10k_c} = \frac{3F}{10k_c} \quad (5)$$

Purlins P2 and P4 were attached to sliding supports with zero reaction force parallel to the purlin direction. Therefore, clips on these purlins exhibited negligible deformation and the displacements of the purlins are equal to the panel rigid body displacement:

$$\delta_2 = \delta_4 = \delta_p = \frac{F}{10k_c} \quad (6)$$

The relationship between the displacements of purlin P3 as compared to the displacement of purlins P2 and P4 is therefore given by:

$$\frac{\delta_3}{\delta_2} = \frac{\delta_3}{\delta_4} = \frac{3F/10k_c}{F/10k_c} = 3 \quad (7)$$

This explains why the displacement of the middle purlin P3 was observed to be approximately three times larger than P2 and P4. This also verifies that almost all of the deformation came from the clips in early part of the loading.

Using the displacement data collected by string potentiometers SP03, SP09 and SP10, clip deformation,  $\delta_{c3}$ , and panel displacement,  $\delta_p$ , could be obtained by  $\delta_{c3} = \text{avg}(\delta_{SP09}, \delta_{SP10})$  and  $\delta_p = \delta_{SP03} - \delta_{c3}$ . Due to panel buckling and rotation of the attachment points on the panels where the string of potentiometers SP09 and SP10 were attached, only the portion of the data collected by these potentiometers at the early stage of the tests (e.g. before middle purlin displacement reached 2 in.) is trusted and included in the plots. As shown in Figure 32, clip deformations were larger than panel displacement at the beginning of the tests, and for most of the specimens the ratio of clip deformation to panel displacement is close to 2, which is the theoretical value given by the ratio of Eq. (2) to Eq. (4). This indicates that the low initial stiffness of the specimens was primarily due to the deformation of the clips.

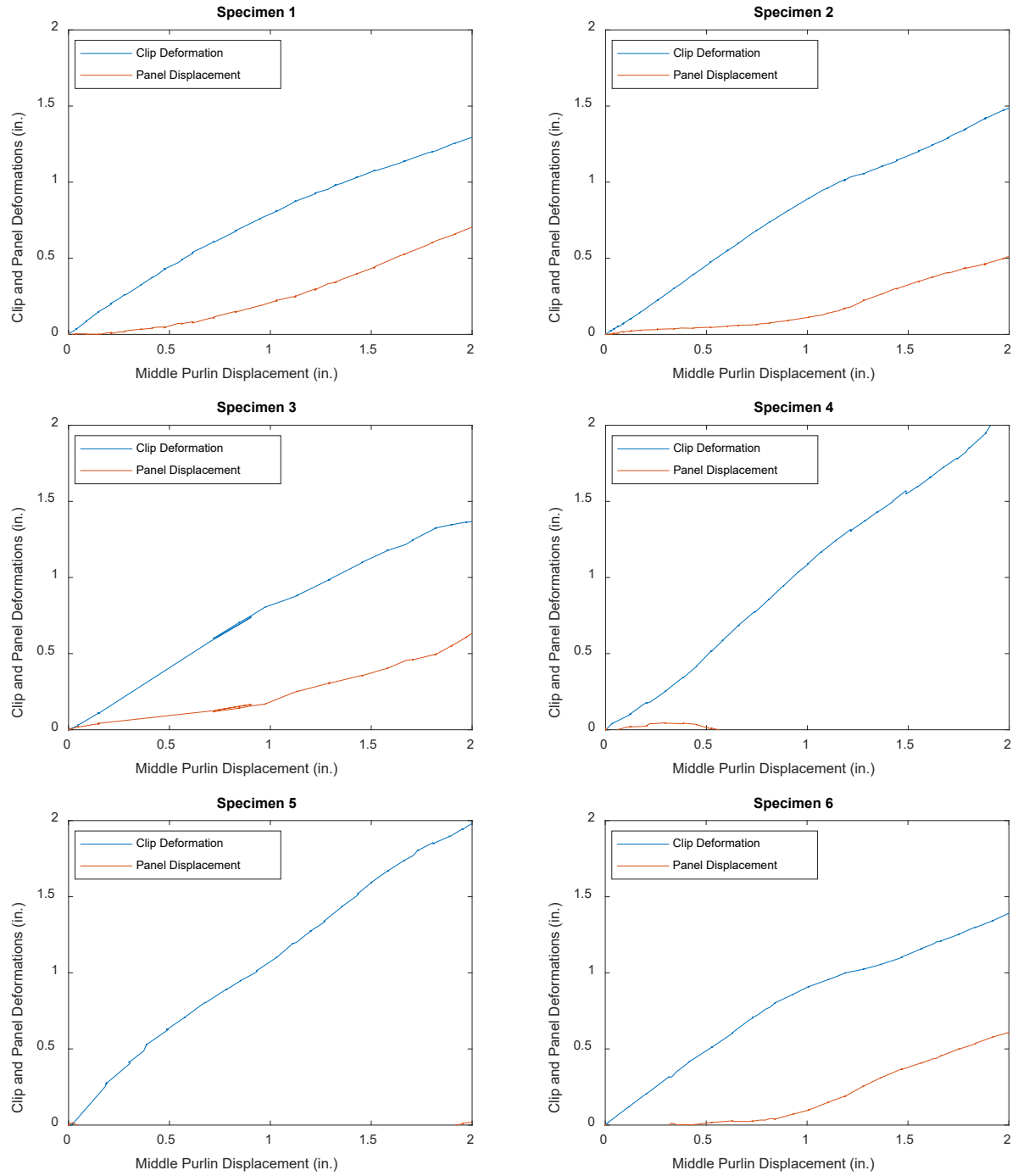


Figure 32 Middle purlin clip and panel deformation curves

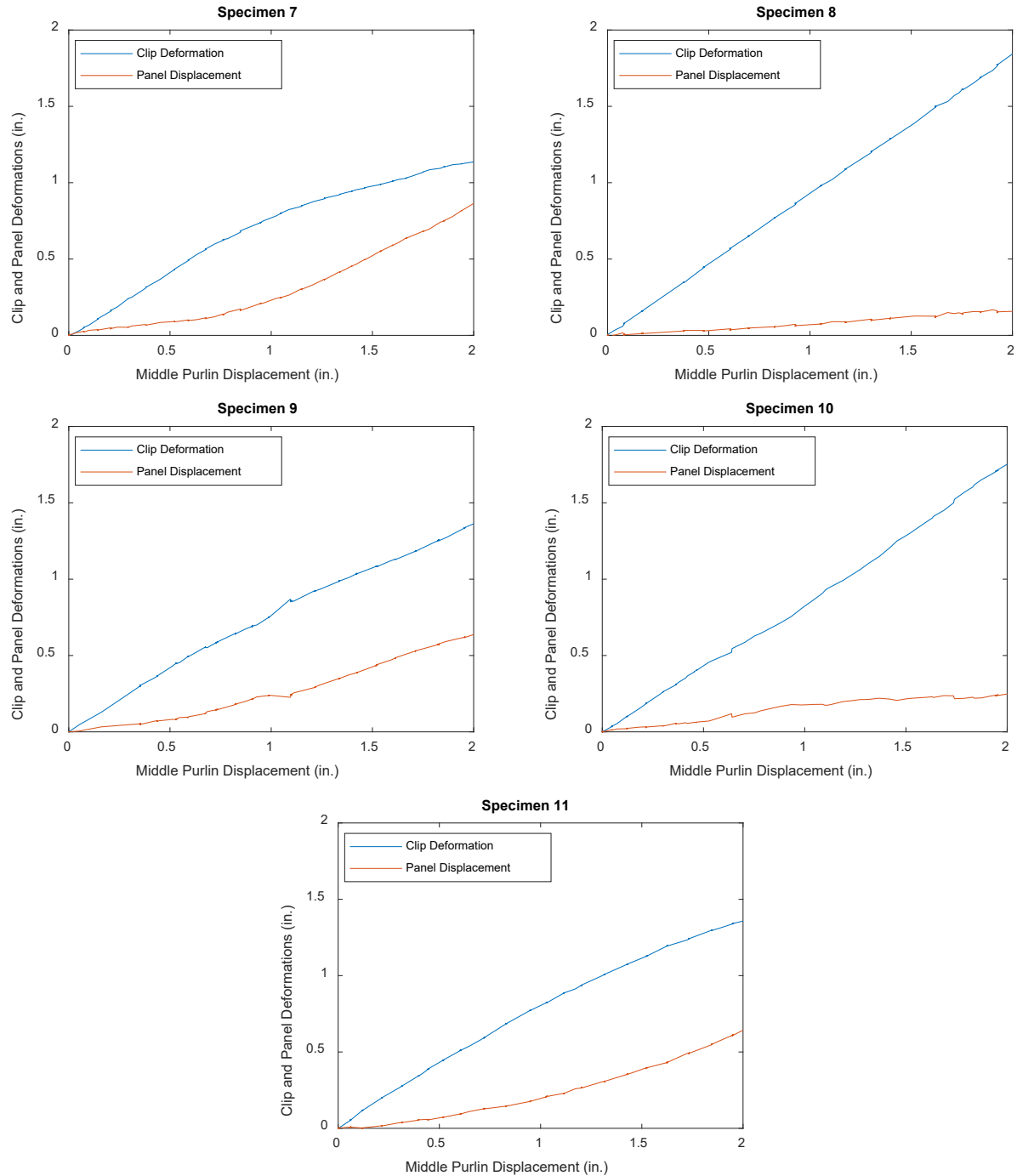


Figure 32 (continued) Middle purlin clip and panel deformation curves

As described in Section 2, the goal of string potentiometers SP06, SP07, and SP08 was to measure the relative slip between adjacent panels. However, because of panel buckling and panel deformations, the data collected using these potentiometers were found to be inaccurate during the parts of the test with large load (Figure 33). Instead, marks were made across the

standing seams between adjacent panels so that panel slip could be visually observed and manually measured. The slip was zero or too small to be observed except for Specimens 5 and 6 which had approximately 0.5 in. panel slip at the exterior purlin location, as is shown in Figure 34.

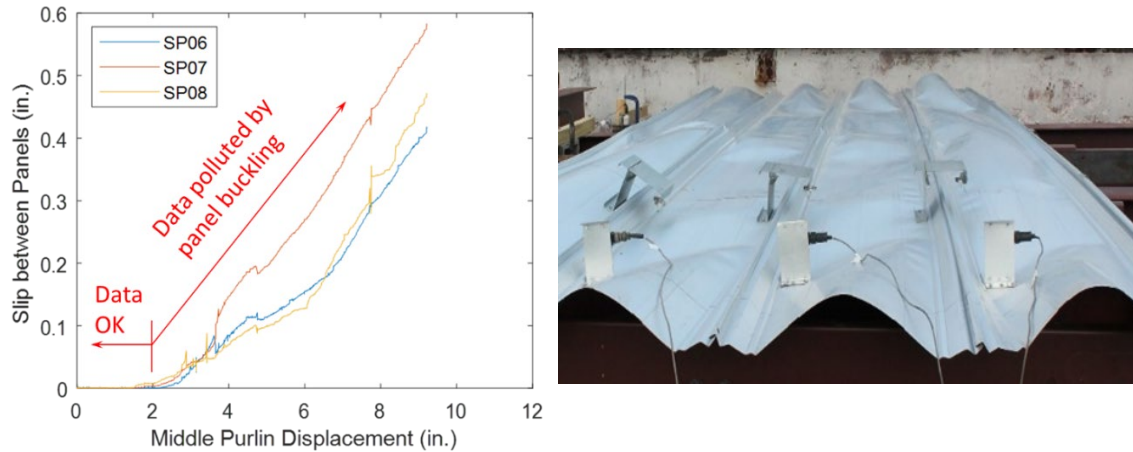


Figure 33 Panel slip measurement affected by panel buckling (from Specimen 2)



Figure 34 Slip between adjacent panels (left: Specimen 4; right: Specimen 5)

To quantify the stiffness,  $K$ , of the specimens, two approaches were used. Typical practice for steel deck diaphragms is to define stiffness as the secant stiffness through a point on the load-deformation curve at 40% of the maximum load. Because many of the specimens had load-deformation curves with very low initial stiffness that increased (due to geometric hardening), this approach leads to stiffness that is not representative of the low initial stiffness. The initial

stiffness was therefore calculated as 1) the secant stiffness through a point on the load-deformation curve at 40% of the maximum load,  $K_{40\%}$ , and 2) the secant stiffness through a point on the load-deformation curve at 1 in. middle purlin displacement,  $K_{1in.}$ . Then, the specimen stiffness,  $K$ , is taken equal to  $K_{40\%}$  for specimens whose middle purlin displacement associated with 40% peak load is smaller than 1 in. (Specimens 4, 5 and 6), and equal to  $K_{1in.}$ , for all other specimens (Specimens 1, 2, 3, 7, 8, 9, 10 and 11). Table 4 provides the values of the maximum load,  $F_{max}$ , and secant stiffnesses of the specimens. Visualization of the secant line used to determine the stiffness of the specimens is provided in the Appendix.

Table 4 Maximum Load and Secant Stiffness of Specimens

Specimen	$F_{max}$ (kip)	$K_{40\%}$ (kip/in)	$K_{1in.}$ (kip/in)	$K$ (kip/in)
1	3.96	0.612	0.505	0.505
2	3.98	0.648	0.145	0.145
3	2.78	0.675	0.545	0.545
4	3.39	8.21	2.74	8.21
5	2.58	2.35	1.73	2.35
6	2.66	2.28	1.62	2.28
7	3.47	0.619	0.478	0.478
8	3.09	0.316	0.087	0.087
9	4.09	0.441	0.402	0.402
10	3.37	0.711	0.879	0.879
11	4.39	0.643	0.573	0.573

### 3.2 Effect of Different Parameters

The effect of different parameters (panel type, clip type, thermal insulation, and purlin spacing) on the strength and stiffness of the specimens is discussed in this section. The secant stiffness  $K$  is used as a representative stiffness in the following discussion.

#### 3.2.1 Panel Type

Table 5 and Figure 35 show the test results for specimens with different panel types. It can be observed that Specimen 4 with vertical rib panel profile had a smaller strength and higher stiffness compared to Specimen 1 with trapezoidal rib panel profile. The specimens with vertical

rib panels exhibited greater stiffness because the vertical ribs better stiffened and restrained the bending deformation of the clips (see Figure 36), and the heights of the ribs and clips were potentially smaller, forcing the clips to deform in tension sooner. The trapezoidal rib panel profile exhibited larger strength because the clips for trapezoidal rib panels had small hooks on the top attached to the panels, which postponed the detachment of clips from the panel seam and contributed to a larger strength compared to the vertical ribs attached to clips without hooks.

Table 5 Maximum Load and Secant Stiffness  $K_{40\%}$  of Specimens with Different Panel Types

Specimen	Panel Profile	Panel Width (in.)	Clip Type	Standoff (in.)	Insulation	Purlin Spacing (ft)	$F_{max}$ (kip)	$K$ (kip/in)
1	Trapezoidal	24	Fixed	0	No	5	3.96	0.505
4	Vertical	16	Fixed	0	No	5	3.39	8.21

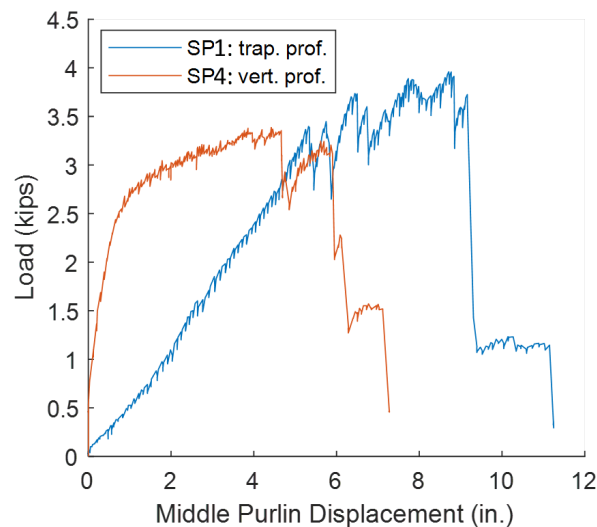


Figure 35 Load-displacement curves of specimens with different panel types

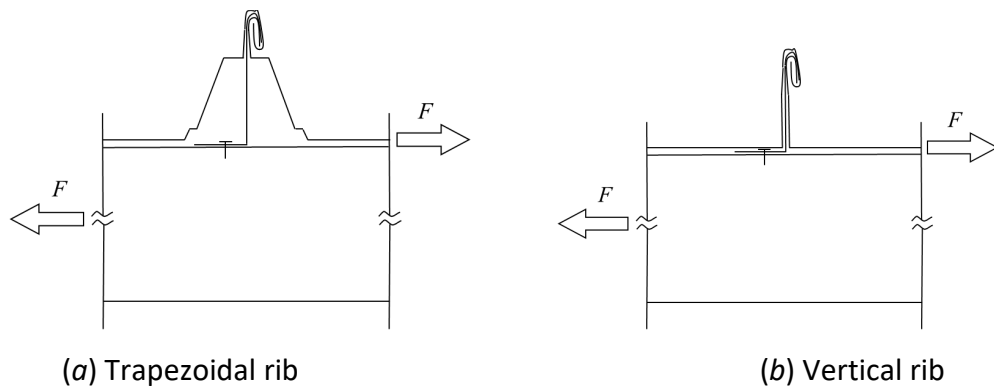


Figure 36 Stiffening and restraint of clips by standing seams with different profiles

### 3.2.2 Clip Type

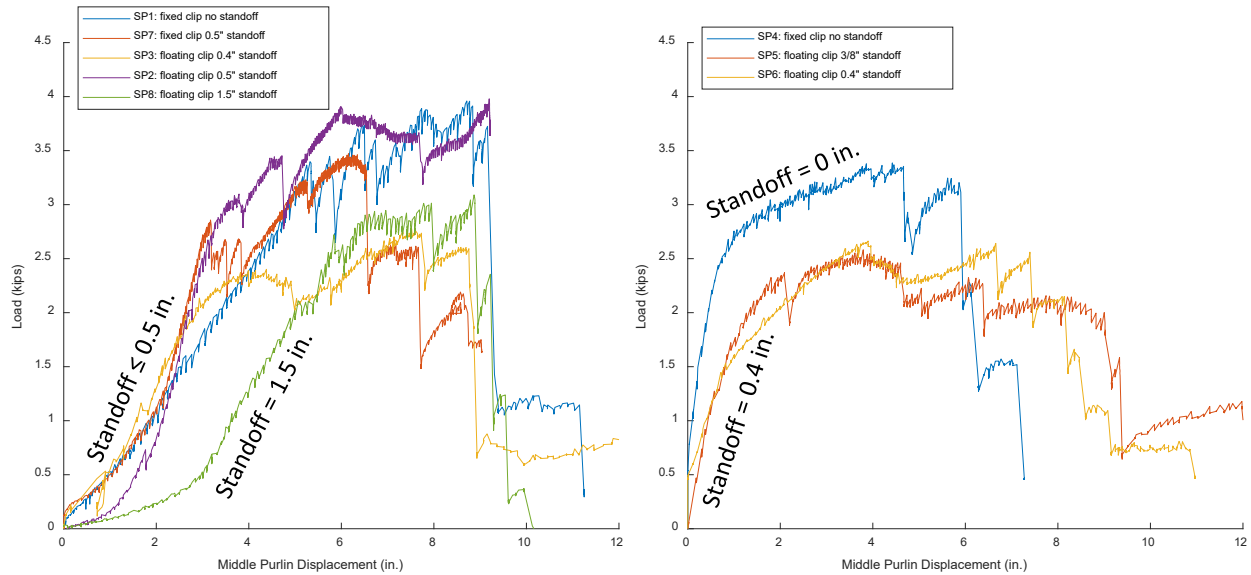
Table 6 and Figure 37 show the test results for specimens with different clip types. For trapezoidal rib panels, fixed clips with standoff of 0 in. or 0.5 in. had similar strength and stiffness. However, for floating clips, the stiffness was sensitive to the clip standoff, and it decreased as the clip standoff increases. This is because a larger clip standoff allows the clips to deform more, leading to a lower stiffness of the specimen.

It is also noted that Specimen 3 had a lower strength and slightly higher stiffness than other specimens with trapezoidal rib panel profile, which may be attributed to its different clip construction. Because the section of the clips in Specimen 3 that was embedded in the seam was smaller, the sliding tab might pull out prematurely, resulting in a reduced strength. However, the bases of the clips were thicker, which may contribute to a higher stiffness.

For vertical rib panels, even 0.4 in. standoff had a large effect on stiffness and Specimens 5 and 6 had less than 30% of the stiffness of Specimen 4 with zero standoff. The amount that the vertical rib restrains clip deformation is less effective if there is a standoff.

Table 6 Maximum Load and Secant Stiffness  $K_{40\%}$  of Specimens with Different Clip Types

Specimen	Panel Profile	Panel Width (in.)	Clip Type	Standoff (in.)	Insulation	Purlin Spacing (ft)	$F_{max}$ (kip)	$K_{40\%}$ (kip/in)
1	Trapezoidal	24	Fixed	0	No	5	3.96	0.505
7	Trapezoidal	24	High Fixed	0.5	No	5	3.47	0.478
3	Trapezoidal	24	Floating	0.4	No	5	2.78	0.545
2	Trapezoidal	24	Floating	0.5	No	5	3.98	0.145
8	Trapezoidal	24	High Floating	1.5	No	5	3.09	0.087
4	Vertical	16	Fixed	0	No	5	3.39	8.21
5	Vertical	16	Floating	3/8	No	5	2.58	2.35
6	Vertical	16	Floating	0.4	No	5	2.66	2.28



(a) Trapezoidal rib panels

(b) Vertical rib panels

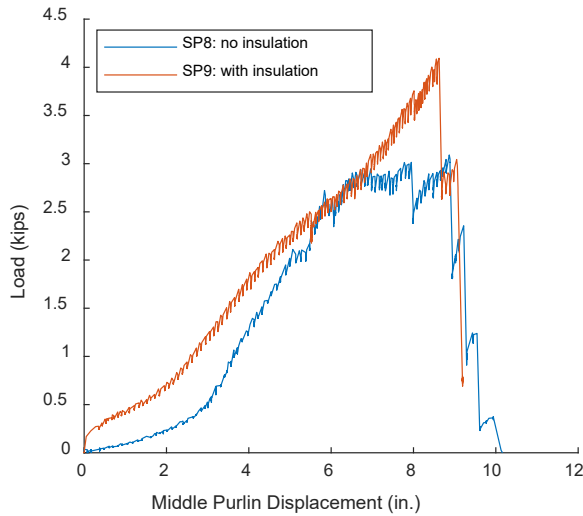
Figure 37 Load-displacement curves of specimens with different clip types

### 3.2.3 Thermal Insulation

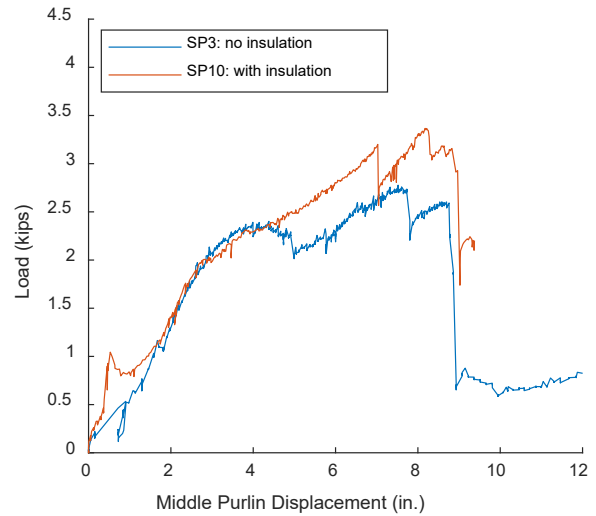
Table 7 and Figure 38 show the test results for specimens with and without thermal insulation. It is observed that including thermal insulation increases the strength and stiffness of the specimens. This is because the thermal blocks and blanket insulation can fill the void below the panel and bring the rib into bearing earlier thereby reducing the clip rotation, which contributed to a larger strength and stiffness of the specimen.

Table 7 Maximum Load and Secant Stiffness  $K_{40\%}$  of Specimens with or without Thermal Insulation

Specimen	Panel Profile	Panel Width (in)	Clip Type	Standoff (in.)	Insulation	Purlin Spacing (ft)	$F_{max}$ (kip)	$K_{40\%}$ (kip/in)
8	Trapezoidal	24	High Floating	1.5	No	5	3.09	0.087
9	Trapezoidal	24	High Floating	1.5	9 in. insulation 1 in. thermal block	5	4.09	0.402
3	Trapezoidal	24	Floating	0.4	No	5	2.78	0.545
10	Trapezoidal	24	Floating	0.4	6 in. insulation no thermal block	5	3.37	0.879



(a) Floating clip with 1.5 in. standoff



(b) Floating clip with 0.4 in. standoff

Figure 38 Load-displacement curves of specimens with or without thermal insulation

### 3.2.4 Purlin Spacing

Figure 39 shows the test results for specimens with different purlin spacing. It can be observed that purlin spacing has a negligible effect on strength and stiffness of the specimens. This is because all of the force transfer occurred between the loaded purlin and the reaction purlins. Additional interior purlins were not found to significantly stiffen the SSR panels against panel buckling.

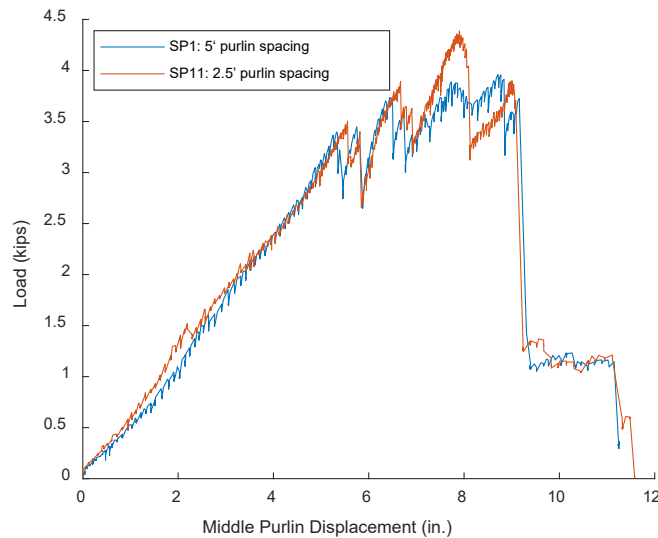


Figure 39 Load-displacement curves of specimens with different purlin spacing

## 4. APPLICATION IN DESIGN AND PRACTICE

### 4.1 Concepts

For metal buildings, tension rod braces (X braces) are typically used to transfer horizontal loads on the roof to the vertical system. The rod bracing coupled with the in-plane stiffness of the SSR system can also provide lateral bracing to the rafters. Figure 40 shows the assumed lateral displacements of a rafter as it undergoes lateral torsional buckling, wherein the rafter is constrained against translation at the intersections of rod bracing with the purlin line. Figure 41 shows a section view of two adjacent rafters undergoing lateral torsional buckling in the same direction. It is assumed that the SSR system provides lateral bracing for rafters between these tension rod bracing points, while the rafter flange braces restrain the twist of the rafter and thus provide torsional bracing.

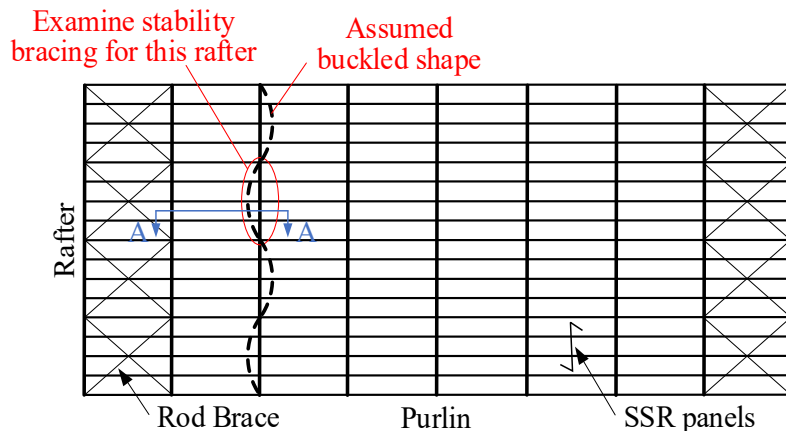


Figure 40 Plan view of typical metal building roof framing with assumed buckled shape of rafter

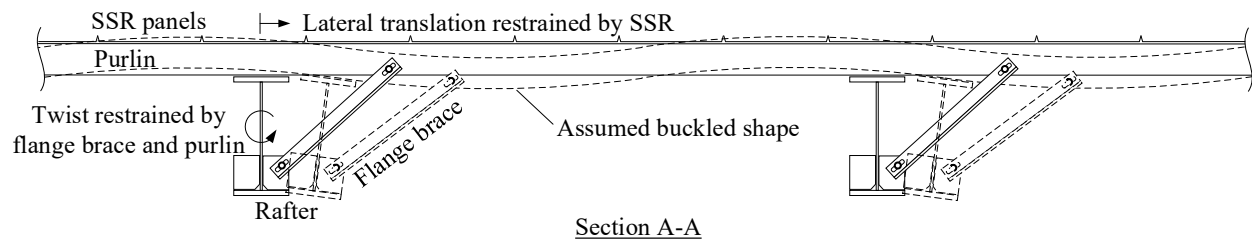


Figure 41 Section view of adjacent rafters braced by SSR and flange braces with assumed buckled shape

AISC 360-16 (AISC 2016a) Appendix 6 specifies the required strength and stiffness for lateral and torsional bracing of beams. The lateral bracing provided by the SSR system is categorized as point bracing at the purlin locations. The required bracing strength,  $P_{Lbro}$ , and the required bracing stiffness,  $\beta_{Lbro}$ , are given as follows:

$$P_{Lbro} = 0.02 \left( \frac{M_r C_d}{h_o} \right) \quad (8)$$

$$\beta_{Lbro} = \frac{1}{\phi} \left( \frac{10 M_r C_d}{L_{br} h_o} \right) \quad (9)$$

where

$M_r$  = required flexural strength of the rafter within the panel under consideration, using LRFD or ASD load combinations

$C_d$  = 1.0, except in the following case:

= 2.0 for the brace closest to inflection point in a beam subject to double curvature bending

$h_o$  = distance between rafter flange centroids

$\phi$  = resistance factor

$L_{br}$  = unbraced length adjacent to the point brace

Torsional bracing of the rafter, provided by the flange braces and purlins, is considered as point bracing. The required bracing strength,  $M_{Tbro}$ , and the required bracing stiffness,  $\beta_{Tbro}$ , are given as follows:

$$M_{Tbro} = 0.02 M_r \quad (10)$$

$$\beta_{Tbro} = \frac{\beta_T}{\left( 1 - \frac{\beta_T}{\beta_{sec}} \right)} \quad (11)$$

where

$$\beta_T = \frac{1}{\phi} \frac{2.4L}{nEI_{yeff}} \left( \frac{M_r}{C_b} \right)^2 \quad (12)$$

$$\beta_{sec} = \text{infinity for a cross-frame like the flange brace-purlin assembly} \quad (13)$$

$E$  = modulus of elasticity of steel = 29,000 ksi

$I_{yeff}$  = effective out-of-plane moment of inertia =  $I_{yc} + (t/c)I_{yt}$

$I_{yc}$  = moment of inertia of the compression flange about the  $y$ -axis

$I_{yt}$  = moment of inertia of the tension flange about the  $y$ -axis

$L$  = length of span

$C_b$  = lateral-torsional buckling modification factor

$c$  = distance from the neutral axis to the extreme compressive fibers

$n$  = number of braced points within the span

$t$  = distance from the neutral axis to the extreme tensile fibers

$\beta_T$  = overall brace system required stiffness

$\beta_{sec}$  = web distortional stiffness, including the effect of web transverse stiffeners, if any

AISC 360-16 states that lateral bracing, torsional bracing, or a combination of the two shall be provided to prevent the relative displacement of the top and bottom flanges (i.e., to prevent twist). Lateral bracing should be attached at or near the beam compression flange to restrain its lateral movement when buckled, meaning that the lateral bracing provided by the SSR can be considered as lateral bracing for positive bending moment (top flange in compression). Since lateral bracing and torsional bracing are provided by the SSR system and flange brace separately, AISC allows combined lateral bracing and torsional bracing using the following interaction equation given in AISC 360-16, Section 6.3 Commentary:

$$\frac{\beta_{Tbr}}{\beta_{Tbro}} + \frac{\beta_{Lbr}}{\beta_{Lbro}} \geq 1.0 \quad (14)$$

where  $\beta_{Tbr}$  and  $\beta_{Lbr}$  are the provided torsional and lateral bracing stiffness, respectively and  $\beta_{Tbro}$  and  $\beta_{Lbro}$  are the required torsional and lateral bracing stiffness, respectively.

For negative bending moment (bottom flange in compression), lateral force from the bottom flange of the buckled rafter is transferred through the flange brace to the purlin. In this case, the flange brace plays two roles: a load path to transfer lateral load from the bottom flange to the SSR for lateral bracing, and a component of a triangular subassembly that supplies torsional bracing to the rafter. AISC 360-16, Section 6.3 Commentary states that when point

torsional bracing is combined with lateral bracing at the tension flange, Eq. (14) applies and, in addition, the torsional brace stiffness should satisfy the following:

$$\beta_{Tbr} \geq \min(\beta_{Lbro} h_o^2, \beta_{Tbro}) \quad (15)$$

where  $\beta_{Lbro}$  is the required lateral bracing stiffness for point bracing as given in Eq. (9).

To examine the requirement for rafter bracing, it is necessary to obtain the bracing strength and stiffness provided by the purlins, SSR panels, and rafter flange braces. Since the strength and initial stiffness of the SSR specimens was dominated by the clips, it is expected that the strength and stiffness will scale proportionally with the number of clips on the purlin. The strength per clip,  $f_c$ , was calculated by dividing the maximum load of the specimens by the number of clips on the middle purlin (5 clips). For stiffness per clip, Eq. (5) is rearranged to solve for the stiffness per clip,  $k_c$ , as given by:

$$k_c = \frac{3F}{10\delta_3} = \frac{3}{10} K \quad (16)$$

where  $K$  is the stiffness of the specimen provided in Table 4.

Table 8 provides the values of the strength and stiffness per clip for the SSR test specimens where strength per clip is the recorded maximum force from the test divided by five clips and the stiffness per clip is calculated using Eq. (16). It is noted that the clips on the edges of the panels (e.g. clips a and e in Figure 13) might not contribute as much to the strength and stiffness of the specimens as the interior clips because they are not as well constrained by the SSR panels. However, they were conservatively treated as identical in the calculations, so the actual strength and stiffness per clip may be slightly larger than reported. For practical application of these results, the closest match of a building's SSR configuration to one of the specimen configurations should be identified, and the lateral bracing strength,  $P_{Lbr}$ , and the stiffness,  $\beta_{Lbr}$ , provided by the SSR can be obtained as follows:

$$P_{Lbr} = n_c f_c \quad (17)$$

$$\beta_{Lbr} = n_c k_c \quad (18)$$

where  $n_c$  is the number of SSR clips on one purlin over a length that is half the distance to adjacent rafters (assumes a tributary width of SSR system used to brace one rafter).

It should be noted that the resulting values for lateral bracing strength and stiffness do not consider the effect of wind and gravity loads. The testing program did not include vertical loads. Uplift associated with wind may cause a reduction in SSR lateral bracing strength because clips are subjected to additional tension and may pull out of the seam when subjected to smaller lateral loads. Conversely, the same uplift may lead to an increase in lateral bracing stiffness because of the geometric stiffening effect. Because the interaction between lateral loading and gravity / uplift loading is not well understood for clips, this interaction is neglected in this work, but recommended for future study.

Table 8 Provided Strength and Stiffness per Clip of SSR for Lateral Bracing of Rafter

Specimen	Configuration						$f_c$ (kip/clip)	$k_c$ (kip/in/ clip)
	Panel Profile	Panel Width	Clip Type	Standoff	Insulation	Purlin Spacing		
1	Trap.	24"	Fixed	0"	No	5'	0.792	0.152
2	Trap.	24"	Floating	0.5"	No	5'	0.796	0.044
3	Trap.	24"	Floating	0.4"	No	5'	0.556	0.164
4	Vert.	16"	Fixed	0"	No	5'	0.678	2.463
5	Vert.	16"	Floating	3/8"	No	5'	0.516	0.705
6	Vert.	16"	Floating	0.4"	No	5'	0.532	0.684
7	Trap.	24"	High Fixed	0.5"	No	5'	0.694	0.143
8	Trap.	24"	High Floating	1.5"	No	5'	0.618	0.026
9	Trap.	24"	High Floating	1.5"	9" insul. 1" therm. blk.	5'	0.818	0.121
10	Trap.	24"	Floating	0.4"	6" insul. no therm. blk.	5'	0.674	0.264
11	Trap.	24"	Fixed	0"	No	2.5'	0.878	0.172

To obtain the torsional bracing strength and stiffness, the subassembly of the purlin, rafter and flange brace is analyzed using a truss analogy as shown in Figure 42. The inflection points in the purlin are assumed to be located at midspan and the rafter is assumed to be axially

rigid. For an applied moment at the top of the rafter,  $M$ , the moment and axial force diagram of the structure is shown in Figure 43. It is noted that this model assumes a flange brace on one side, but a similar approach could be followed to determine bracing stiffness for flange braces on both sides of the rafter.

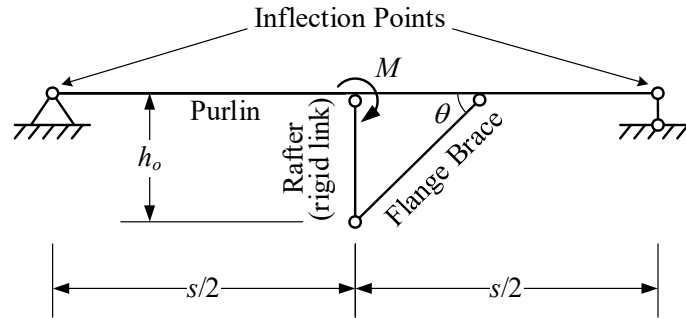


Figure 42 Structure assemblage for analyzing torsional bracing strength and stiffness of rafter provided by flange brace and purlin

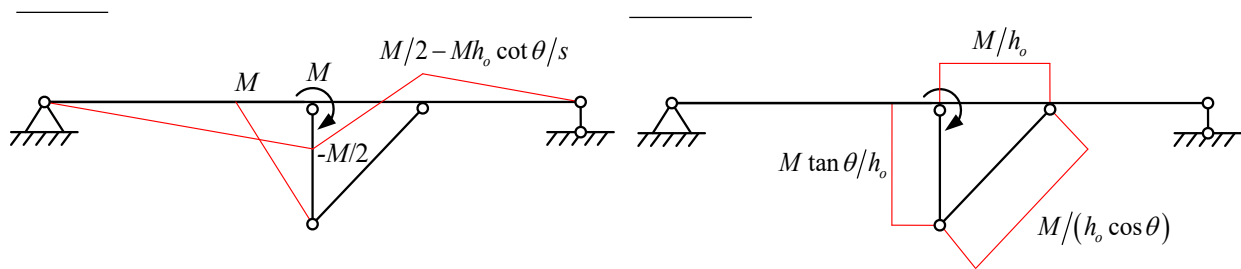


Figure 43 Moment and axial force diagram of the assemblage subjected to concentrated moment applied at the top of rafter

The strength of the torsional bracing provided by the flange brace and the purlin, i.e., the maximum moment that can be applied, is reached when the limit state of any component occurs. The torsional bracing strength can therefore be obtained by setting the maximum moment acting on the purlin equal to its flexural strength and by setting the maximum axial force experienced by the purlin and flange brace equal to their compressive strength (note that the applied moment can be reversed, and that the compressive strength is typically smaller than the tensile strength), which is also limited by the connections of the flange brace to the rafter and purlin, and is given by:

$$M_{Tbr} = \min\left(2M_{a,p}, P_{n,p} h_o, P_{n,b} h_o \cos \theta, V_{n,bolt} h_o \cos \theta\right) \quad (19)$$

where  $M_{a,p}$  is the available flexural strength of the purlin to resist rafter bracing loads (after consideration of gravity and wind loads),  $P_{n,p}$  is the compressive strength of the purlin between the points of rafter and flange brace attachments,  $P_{n,b}$  is the compressive strength of the flange brace, and  $V_{n,bolt}$  is the nominal shear strength of the bolted connections (due to bolt shear, bearing, and tear-out) at the ends of flange brace.

The torsional bracing stiffness is found by determining the rafter twist,  $\phi$ , associated with an arbitrary applied moment,  $M$ . Using the principle of virtual work, the rotation of the rafter section when subjected to the applied moment,  $M$ , can be obtained as follows:

$$\phi = \frac{M}{EI_p} \left( \frac{s}{12} + \frac{h_o^2}{3s \tan^2 \theta} - \frac{h_o}{6 \tan \theta} \right) + \frac{M}{EA_p h_o \tan \theta} + \frac{M}{EA_b h_o \cos^2 \theta \sin \theta} \quad (20)$$

where  $I_p$  is the moment of inertia of the purlin,  $A_p$  is the cross-section are of the purlin, and  $A_b$  is the cross-section area of the flange brace.

Therefore, the torsional bracing stiffness provided by the flange brace and the purlin is given by:

$$\beta_{Tbr} = \frac{M}{\phi} = \frac{E}{\frac{1}{I_p} \left( \frac{s}{12} + \frac{h_o^2}{3s \tan^2 \theta} - \frac{h_o}{6 \tan \theta} \right) + \frac{1}{A_p h_o \tan \theta} + \frac{1}{A_b h_o \cos^2 \theta \sin \theta}} \quad (21)$$

Eq. (21) provides a theoretical estimate of the torsional bracing stiffness based on the flange brace configuration shown in Figure 42. It is noted that this equation is based on an idealized configuration and does not consider double flange braces or some sources of flexibility (e.g. connection flexibility). However, a similar procedure could be followed to obtain the torsional bracing stiffness for two-sided flange bracing systems or systems with additional sources of flexibility.

To summarize, checking the adequacy of the rafter lateral bracing can be conducted in two steps as follows:

1. Check the lateral bracing initial stiffness. Calculate the required lateral bracing stiffness,  $\beta_{Lbro}$ , and required torsional bracing stiffness,  $\beta_{Tbro}$ , using Eq. (9) and Eq. (11), respectively. Calculate the provided lateral bracing stiffness,  $\beta_{Lbr}$ , and provided torsional bracing stiffness,  $\beta_{Tbr}$ , using Eq. (18), and Eq. (21) (or equivalent approach), respectively. Substitute these four values into Eq. (14), and the resulting interaction inequality needs to be satisfied. For negative bending, Eq. (15) also needs to be satisfied.
2. Check the lateral bracing strength. Calculate the required lateral bracing strength,  $P_{Lbro}$ , and required torsional bracing strength,  $M_{Tbro}$ , using Eq. (8) and Eq. (10), respectively. Calculate the provided lateral bracing strength,  $P_{Lbr}$ , and provided torsional bracing strength,  $M_{Tbr}$ , using Eq. (17), and Eq. (19), respectively. One of the following two inequalities needs to be satisfied:  $P_{Lbr} > P_{Lbro}$  or  $M_{Tbr} > M_{Tbro}$ .

## 4.2 Example

A prototype metal building designed by MBMA (NBM 2018) located in Orlando, Florida is selected to calculate typical values of required strength and stiffness for rafter bracing. Figure 44 shows the roof framing details of the prototype metal building. Rafter dimensions are: flange width  $b_f = 6$  in., thickness  $t_f = 0.25$  in., web depth  $h = 25$  in., and web thickness  $t_w = 0.1345$  in. Rod brace spacing is 20 ft and purlin spacing is 5 ft. The SSR system has a similar configuration (panel type, clip type, etc.) to that of Specimen 1 in Table 8. The moment of inertia of the purlins  $I_p = 10.15$  in.<sup>4</sup>. Bracing requirements for the rafter segment between grid lines 2-3 and E-G is evaluated in this section. It should be noted that this example only provides the check for the particular rafter segment of interest and positive moment is assumed. In practice, it would be necessary to check each bracing span individually considering all the stability requirements. Also, this example uses LRFD, but a similar procedure could be used with ASD.

Assuming that the middle portion of the rafter is buckling between the points where the diagonal rod bracing attach to the rafter (i.e. identified as “rafter segment of interest” in Figure 44), the unbraced length for rafter lateral bracing is the spacing of purlins,  $L_{br} = 5$  ft. This is consistent with the definition of  $L_{br}$  for point bracing in AISC 360-16 Section 6.1 commentary. It

is noted that the test setup used a span equal to 20 ft (corresponding to  $L_{br} = 10$  ft), but because the initial stiffness of the specimens was dominated by clip deformation and not SSR panel deformations, the initial stiffness is expected to be similar if the span were half as long.

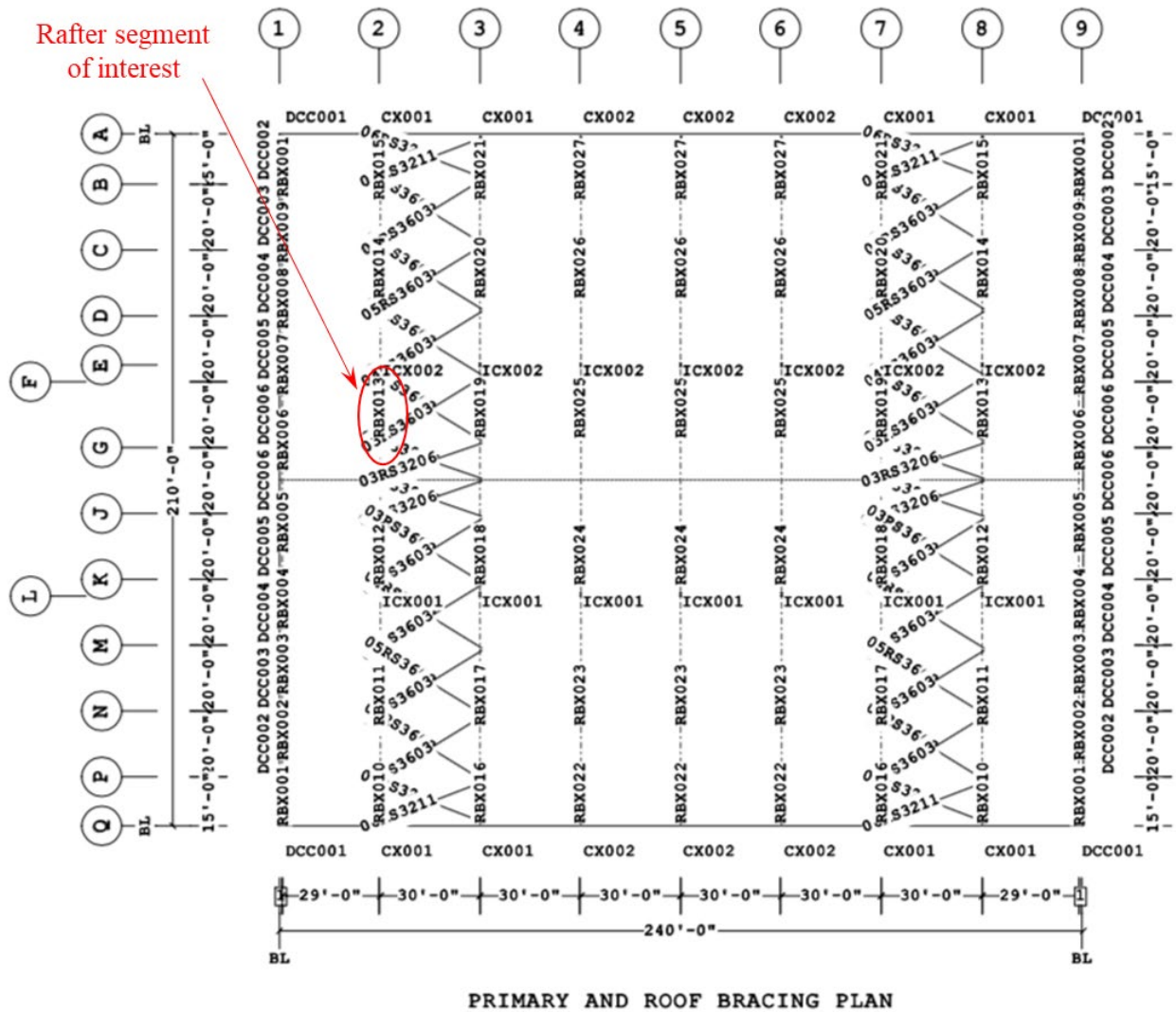


Figure 44 Plan view of roof framing detail of prototype metal building

It is assumed that the moment demand is  $M_r = M_y = 2818$  kip-in for the rafter with compression at the top flange. With  $C_d = 1.0$ , and  $h_o = 25.25$  in., the required strength of rafter lateral bracing is given by:

$$P_{Lbro} = 0.02 \left( \frac{M_r C_d}{h_o} \right) = 0.02 \left( \frac{(2818 \text{ kip-in.})(1.0)}{25.25 \text{ in.}} \right) = 2.2 \text{ kip} \quad (22)$$

The required stiffness of rafter lateral bracing is given by:

$$\beta_{Lbro} = \frac{1}{\phi} \left( \frac{10M_r C_d}{L_{br} h_o} \right) = \frac{1}{0.75} \left( \frac{10(2818 \text{ kip-in.})(1.0)}{(5 \text{ ft})(12 \text{ in./ft})(25.25 \text{ in.})} \right) = 24.8 \text{ kip/in.} \quad (23)$$

The required flexural strength of rafter torsional bracing is given by:

$$M_{Tbro} = 0.02M_r = 0.02(2818 \text{ kip-in.}) = 56.4 \text{ kip-in.} \quad (24)$$

For the selected rafter segment, values of the following quantities can be obtained:  $I_{yeff} = I_y = 9 \text{ in.}^4$  for doubly symmetric section,  $L = 20 \text{ ft}$ ,  $n = 3$ . A uniform moment is assumed with  $C_b = 1.0$  which leads to  $\beta_T = 7790 \text{ kip-in.}$  The flange brace and purlin can be considered as a cross frame and therefore the stiffness of the rafter web does not reduce the torsional bracing stiffness, i.e.  $\beta_{sec} = \text{infinity}$ . Therefore,

$$\beta_{Tbro} = \beta_T = 7790 \text{ kip-in.} \quad (25)$$

As is shown in Figure 44, the spacing of rafters is 30 ft. The spacing of the clips on the purlins is equal to the panel width (24 in.), and thus there are  $n_c = (30 \text{ ft})(12 \text{ ft/in.})/(24 \text{ in.}) = 15$  clips on each purlin within one rafter spacing. Using the values for Specimen 1 in Table 8, the lateral bracing strength and stiffness provided by the SSR is given by:

$$P_{Lbr} = n_c f_c = (15)(0.792 \text{ kip/ft}) = 11.9 \text{ kip} \quad (26)$$

$$\beta_{Lbr} = n_c k_c = (15)(0.152 \text{ kip/in./ft}) = 2.28 \text{ kip/in.} \quad (27)$$

Assume that the flange brace is at an angle of  $\theta = 45^\circ$  and the flange brace consists of an L2×2×1/8. From the AISC Steel Construction Manual (AISC 2016b) and the AISI Cold-Formed Steel Design Manual (AISI 2017) we have:  $M_{n,p} = 124 \text{ kip-in.}$ ,  $P_{n,p} = 57.8 \text{ kip}$ ,  $P_{n,b} = 10.7 \text{ kip}$ , where  $M_{n,p}$  is the nominal flexural strength of the purlin. For this example, the flexural strength of the purlin available to resist rafter bracing loads after consideration of gravity and wind loads is given as,  $M_{a,p} = 37.2 \text{ kip-in}$  (calculations not shown here). It is also assumed that limit states

associated with the bolted connections on the two ends of flange brace do not control (which may not be typical). Therefore,

$$\begin{aligned}
 M_{Tbr} &= \min(2M_{a,p}, P_{n,p}h_o, P_{n,b}h_o \cos \theta) \\
 &= \min[2(37.2 \text{ kip-in.}), (57.8 \text{ kip})(25.25 \text{ in.}), (10.7 \text{ kip})(25.25 \text{ in.})(\cos 45^\circ)] \quad (28) \\
 &= 74.4 \text{ kip-in.}
 \end{aligned}$$

The torsional bracing stiffness provided by the flange brace and the purlin is given by:

$$\begin{aligned}
 \beta_{Tbr} &= \frac{E}{\frac{1}{I_p} \left( \frac{s}{12} + \frac{h_o^2}{3s \tan^2 \theta} - \frac{h_o}{6 \tan \theta} \right) + \frac{1}{A_p h_o \tan \theta} + \frac{1}{A_b h_o \cos^2 \theta \sin \theta}} \\
 &= 29000 \text{ ksi} \left[ \frac{1}{10.15 \text{ in.}^4} \left( \frac{360 \text{ in.}}{12} + \frac{(25.25 \text{ in.})^2}{3(360 \text{ in.})(\tan^2 45^\circ)} - \frac{25.25 \text{ in.}}{6(\tan 45^\circ)} \right) \right. \\
 &\quad \left. + \frac{1}{(1.05 \text{ in.}^2)(25.25 \text{ in.})(\tan 45^\circ)} + \frac{1}{(0.491 \text{ in.}^2)(25.25 \text{ in.})(\cos^2 45^\circ)(\sin 45^\circ)} \right] \quad (29) \\
 &= 10122 \text{ kip-in.}
 \end{aligned}$$

Check the adequacy of the rafter bracing:

1. Check the rafter bracing stiffness. The requirement is given as follows:

$$\frac{\beta_{Tbr}}{\beta_{Tbro}} + \frac{\beta_{Lbr}}{\beta_{Lbro}} > 1.0$$

$$\frac{10122 \text{ kip-in.}}{7790 \text{ kip-in.}} + \frac{2.3 \text{ kip/in.}}{24.8 \text{ kip/in.}} = 1.39$$

$$1.39 > 1.0 \quad \text{OK}$$

Since this portion of the rafter is subjected to positive bending, the additional check on torsional bracing stiffness associated with negative bending is not required.

2. Check the rafter bracing strength. The requirement is that one of the following two inequalities must be satisfied:

$$P_{Lbr} \geq P_{Lbro}$$

$$11.9 \text{ kip} \geq 2.2 \text{ kip} \quad \text{OK}$$

$$M_{Tbr} \geq M_{Tbro}$$

$$74.4 \text{ kip-in.} \geq 56.4 \text{ kip-in.} \quad \text{OK}$$

The provided rafter bracing is therefore adequate.

It should be noted that this example only provides the check of bracing requirements for the particular rafter segment of interest. In practice, it would be necessary to check each bracing span individually.

### 4.3 Discussion

Based on the example calculations provided in Section 4.2, it is found that the lateral bracing provided by the SSR assembly can contribute to bracing the rafter against lateral torsional buckling. Rafter bracing can be provided by a combination of torsional bracing from rafter flange bracing and lateral bracing from the SSR assembly. This consideration of SSR assembly in the rafter bracing calculations may allow the frequency or size of the flange braces to be reduced. In some cases, such as SSR configurations with vertical rib panels and zero standoff clips, it may be possible to eliminate flange braces in the positive moment region of the rafter.

It is noted that the lateral bracing strength and stiffness provided by the SSR system is based on the results of the experimental study which did not include vertical loads associated with gravity loads or wind loads. As described in Section 4.1, gravity loads and wind loads may affect the lateral bracing stiffness and strength associated with each clip. The interaction between vertical loads and lateral bracing loads deserves further study.

## 5. CONCLUSIONS AND RECOMMENDATIONS

### 5.1 Conclusions

In this study, 11 SSR specimens with different configurations (panel type, clip type, thermal insulation, and purlin spacing) were tested to investigate the ability of SSR panels to restrain the longitudinal movement of the purlins thus providing lateral bracing for rafters and preventing lateral torsional buckling. Based on the analysis of test results, the following observations were made:

- 1) The in-plane stiffness of an SSR system is governed primarily by bending of the clips that connect the SSR panels to the purlins.
- 2) Specimens with vertical rib panels exhibit significantly higher stiffness than those with trapezoidal rib panels because the vertical ribs provide some restraint against clip bending (i.e., shorter clear height of clip for bending). For instance, a specimen with vertical rib panels had 16 times larger stiffness than a similar specimen with trapezoidal ribs (Specimen 4 vs. Specimen 1).
- 3) The clip standoff dimension can have a substantial effect on SSR system stiffness. For trapezoidal rib panels, specimens with fixed clips and a zero or 0.5 in. clip standoff had similar stiffness (Specimens 1 and 7), but with floating clips the stiffness decreased as the clip standoff increased (Specimens 2, 3 and 8). For vertical rib panels, even a small increase in standoff can cause a substantial drop in stiffness as demonstrated by a 3.5 times drop in stiffness as the standoff is increased from 0 in. to 0.4 in. (Specimen 4 vs. Specimens 5 and 6).
- 4) Thermal blocks and blanket insulation can increase the stiffness of the SSR system. Addition of 9 in. insulation and 1 in. thermal blocks had 4.5 times larger stiffness for specimens with 1.5 in. standoff high floating clips (Specimen 9 vs. Specimen 8) , and the use of 6 in. insulation (no thermal block) led to 60% increase in stiffness for specimens with shorter 0.4 in. standoff floating clips (Specimen 10 vs. Specimen 3).
- 5) For the test setup used in this study, the purlin spacing was shown to have negligible effect on strength or stiffness of the specimens.

An approach for evaluating lateral bracing requirements of a rafter considering both the flange braces and SSR lateral bracing was identified based on AISC 360-16. The requirement for rafter lateral bracing can be satisfied by a combination of torsional bracing provided by rafter flange bracing and lateral bracing from the SSR system. If SSR panels are present on the roof, which is typical in metal buildings, considering the SSR panels may allow the frequency or size of the flange braces to be reduced. In some cases, it may even be possible to eliminate flange braces in the positive moment regions of the rafter if the SSR roof provides enough lateral bracing stiffness and strength.

## **5.2 Recommendations for Future Work**

It is recommended that more experimental tests be conducted to further characterize the effect of different parameters on the in-plane strength and stiffness of SSR systems. Parameters that should be considered include: panel type (trapezoidal vs. vertical), panel width, panel thickness, manufacturer, clip type (fixed vs. floating), standoff dimension, and tightness of the seam as measured by pressure used in seaming or resulting seam thickness, among which the panel type and clip configuration may be the most influential parameters based on the limited test results from this study. The current experimental program examined eleven specific SSR assemblies, but does not give sufficient information about the many SSR combinations that are possible. Further work is required to produce generalized tables of stiffness and strength that are applicable to a broad range of SSR assemblies. Also, in future experimental programs, multiple repetitions should be included to examine the variability in results. Since the in-plane stiffness of SSR systems has been shown in the current tests to be governed almost exclusively by clip deformations and the strength of the system is associated with clip failure or clip pull-out, it may be possible to conduct (or leverage existing data from) small-scale tests on individual clips to characterize system stiffness and strength. For these types of small-scale tests to be useful, it should be verified that they can capture the clip deformation and failure modes observed in this study. Furthermore, the effect of gravity and uplift loads on the ability of the clips to resist lateral bracing loads requires further investigation. Lastly, a study is warranted on the purlin and flange brace assembly to investigate the effects of far-side and near-side flange braces for rafters, the

angle of the flange braces, lapped purlins over the rafter, and the effect of gravity/uplift loads on the overall strength and stiffness of the assembly.

## REFERENCES

- AISC. (2016a). *AISC 360-16, Specification for Structural Steel Buildings*. American Institute of Steel Construction, Chicago, IL.
- AISC. (2016b). *Steel construction manual* (15th ed.). American Institute of Steel Construction, Chicago, IL.
- AISI. (2017). *AISI D100 - 17, Cold - Formed Steel Design Manual, 2017 Edition*. American Iron and Steel Institute, Washington, D.C.
- NBM Technologies Inc. (2018). Evaluation of Metal Building System Seismic Response Modification Coefficients. NBM Technologies Inc., Blacksburg, VA.

## APPENDIX

This appendix provides more information of the test results for each specimen, including plots of load-displacement curves, purlin displacements, clip and panel deformations on middle purlins, and pictures of deformed shape and damage of the specimens.

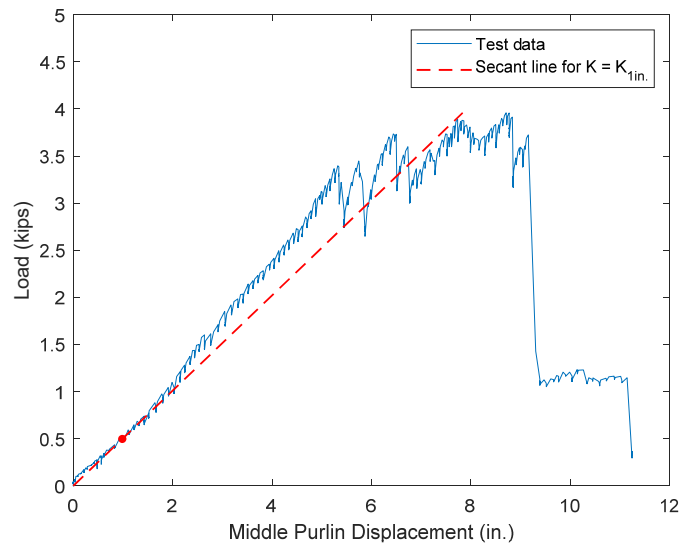


Figure A1-1 Load-displacement curve for Specimen 1

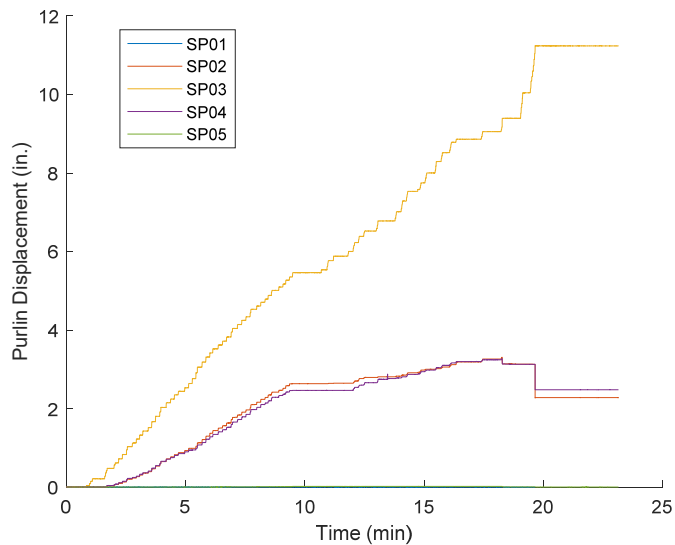


Figure A1-2 Purlin displacements of Specimen 1



Figure A1-3 Deformed shape of Specimen 1



Figure A1-4 Clip damage of Specimen 1

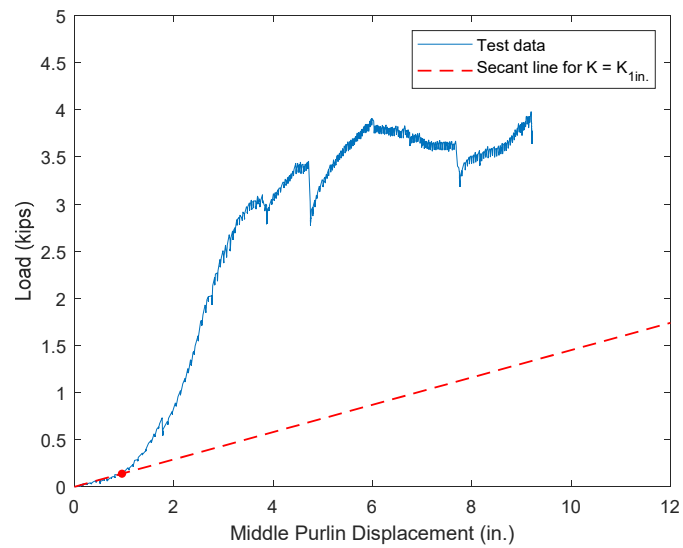


Figure A2-1 Load-displacement curve for Specimen 2

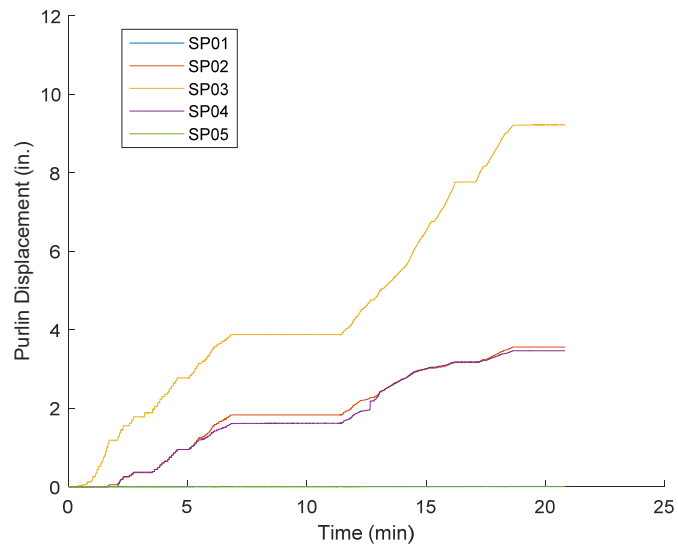


Figure A2-2 Purlin displacements of Specimen 2



Figure A2-3 Deformed shape of Specimen 2



Figure A2-4 Clip damage of Specimen 2

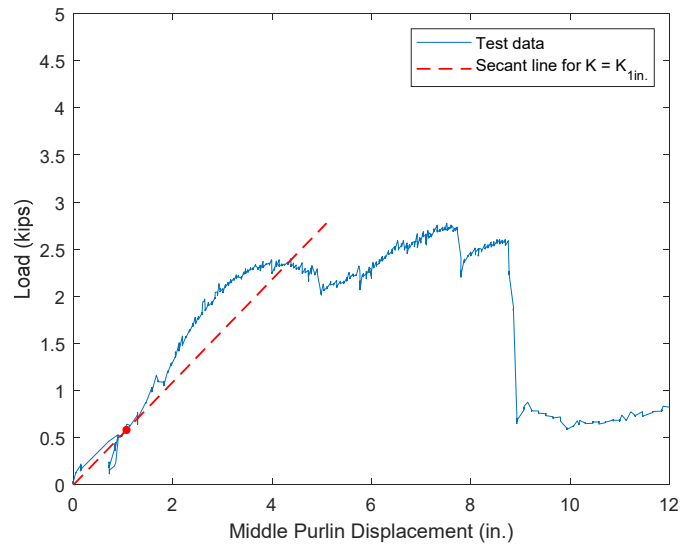


Figure A3-1 Load-displacement curve for Specimen 3

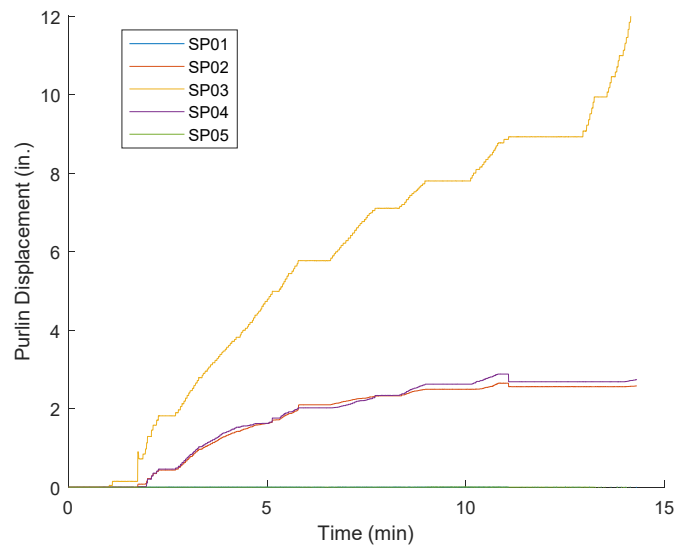


Figure A3-2 Purlin displacements of Specimen 3



Figure A3-3 Deformed shape of Specimen 3



Figure A3-4 Clip damage of Specimen 3

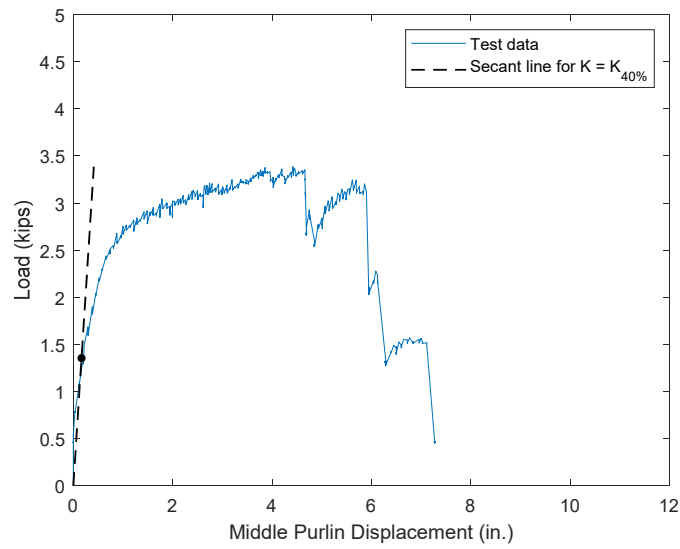


Figure A4-1 Load-displacement curve for Specimen 4

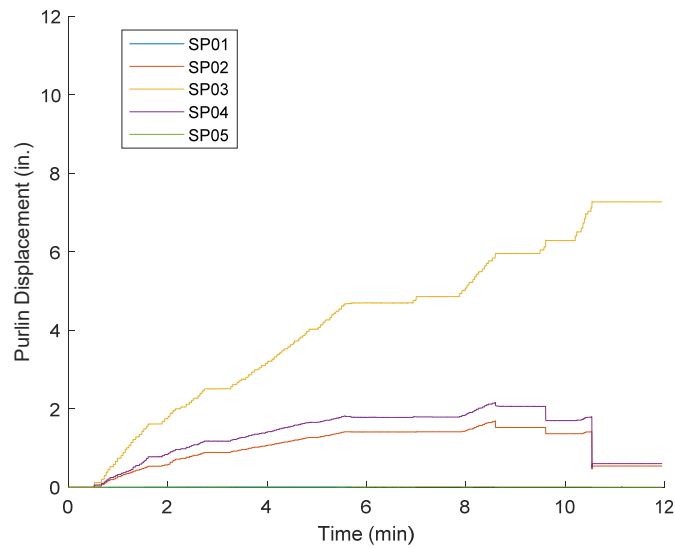


Figure A4-2 Purlin displacements of Specimen 4



Figure A4-3 Deformed shape of Specimen 4



Figure A4-4 Clip damage of Specimen 4

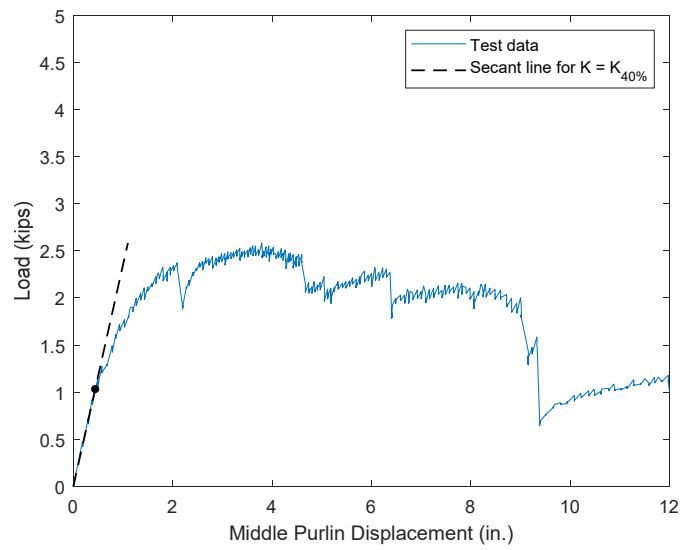


Figure A5-1 Load-displacement curve for Specimen 5

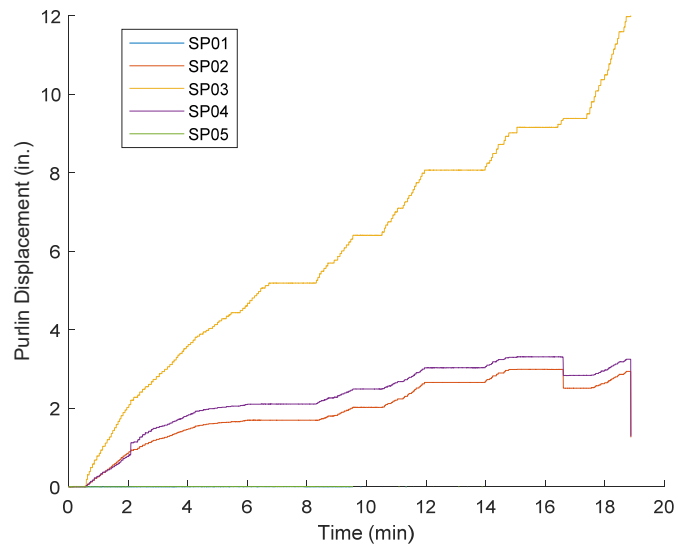


Figure A5-2 Purlin displacements of Specimen 5



Figure A5-3 Deformed shape of Specimen 5



Figure A5-4 Clip damage of Specimen 5

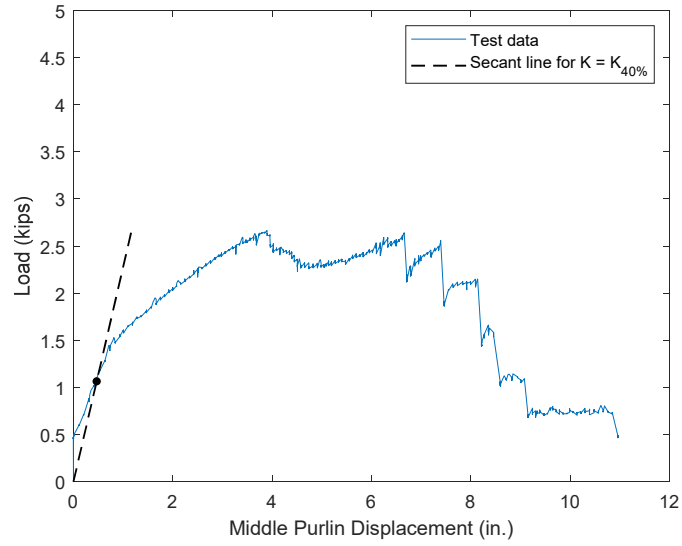


Figure A6-1 Load-displacement curve for Specimen 6

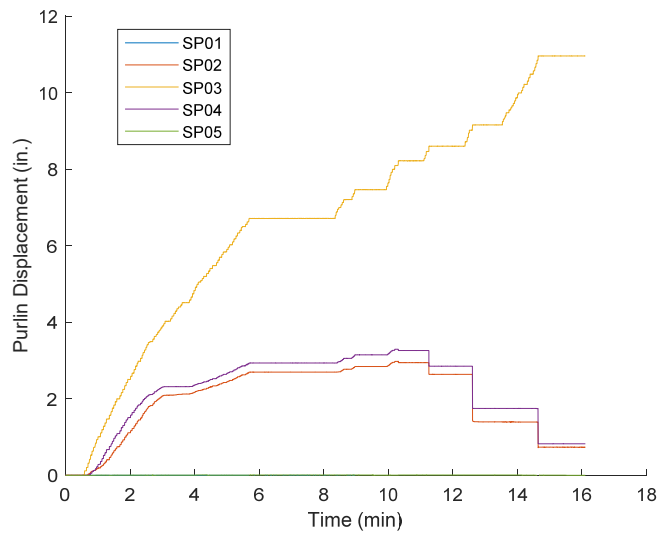


Figure A6-2 Purlin displacements of Specimen 2



Figure A6-3 Deformed shape of Specimen 6



Figure A6-4 Clip damage of Specimen 6

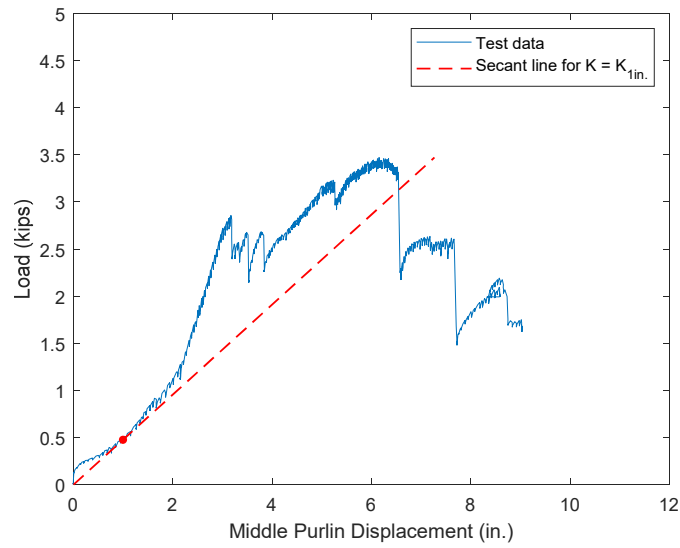


Figure A7-1 Load-displacement curve for Specimen 7

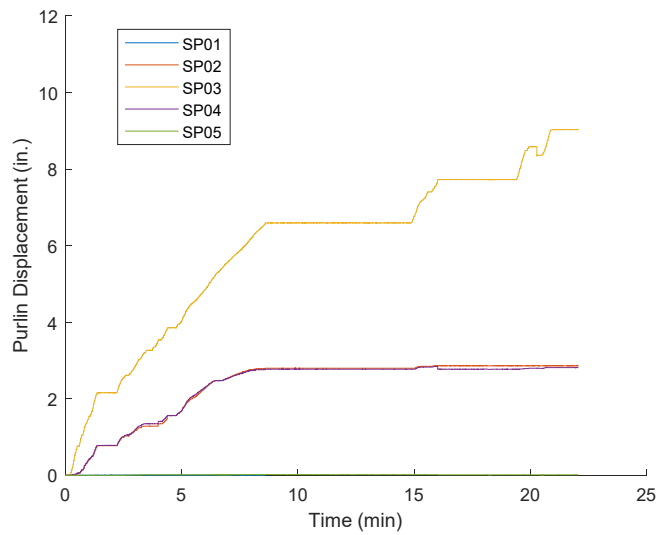


Figure A7-2 Purlin displacements of Specimen 7



Figure A7-3 Deformed shape of Specimen 7



Figure A7-4 Clip damage of Specimen 7

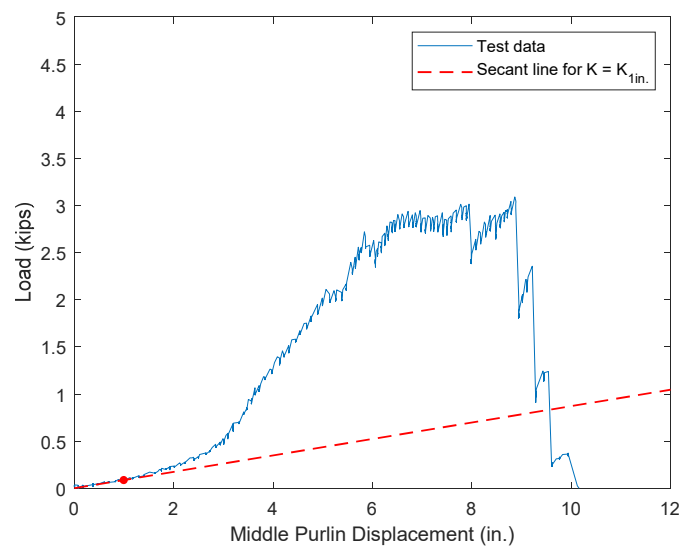


Figure A8-1 Load-displacement curve for Specimen 8

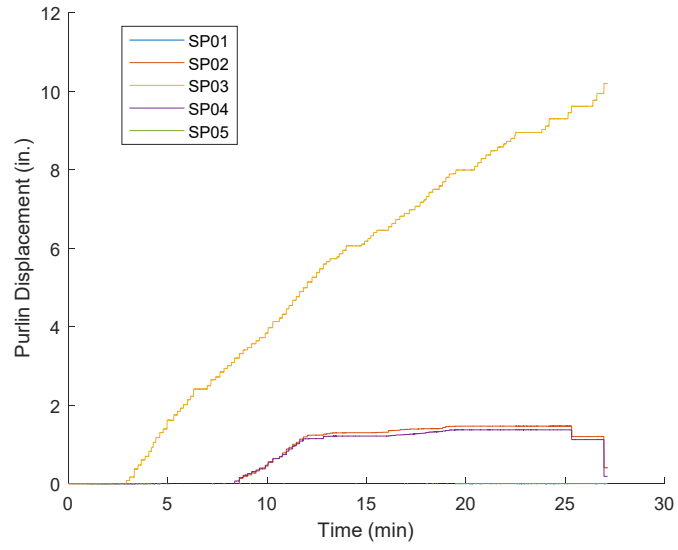


Figure A8-2 Purlin displacements of Specimen 8



Figure A8-3 Deformed shape of Specimen 8



Figure A8-4 Clip damage of Specimen 8

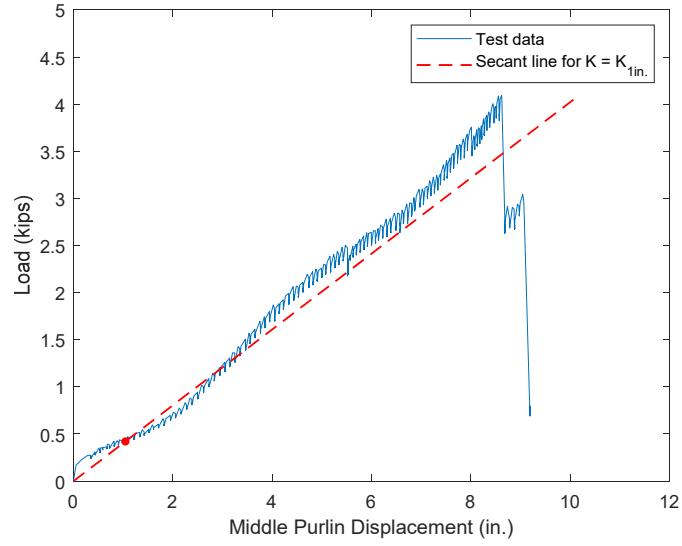


Figure A9-1 Load-displacement curve for Specimen 9

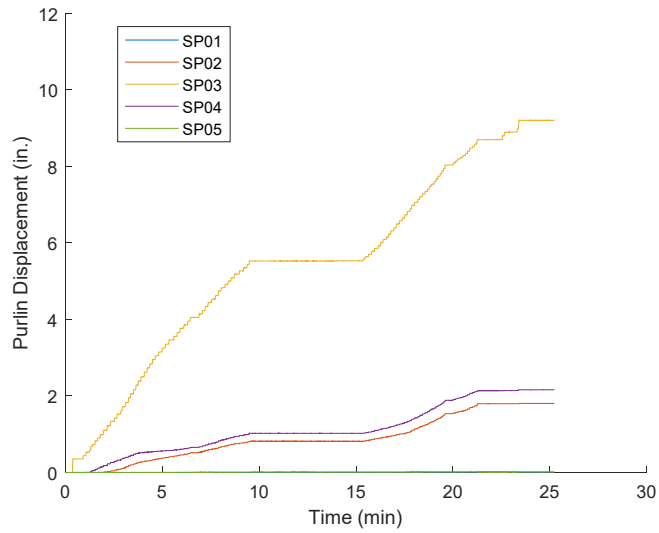


Figure A9-2 Purlin displacements of Specimen 9



Figure A9-3 Deformed shape of Specimen 9



Figure A9-4 Clip damage of Specimen 9

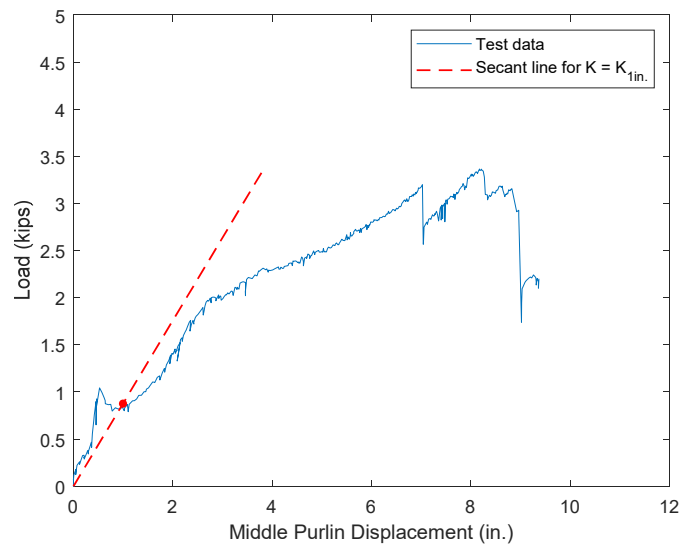


Figure A10-1 Load-displacement curve for Specimen 10

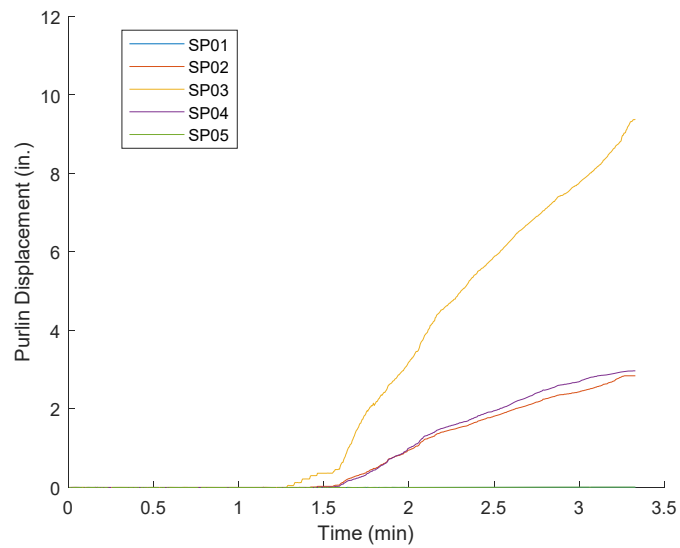


Figure A10-2 Purlin displacements of Specimen 10



Figure A10-3 Deformed shape of Specimen 10



Figure A10-4 Clip damage of Specimen 10

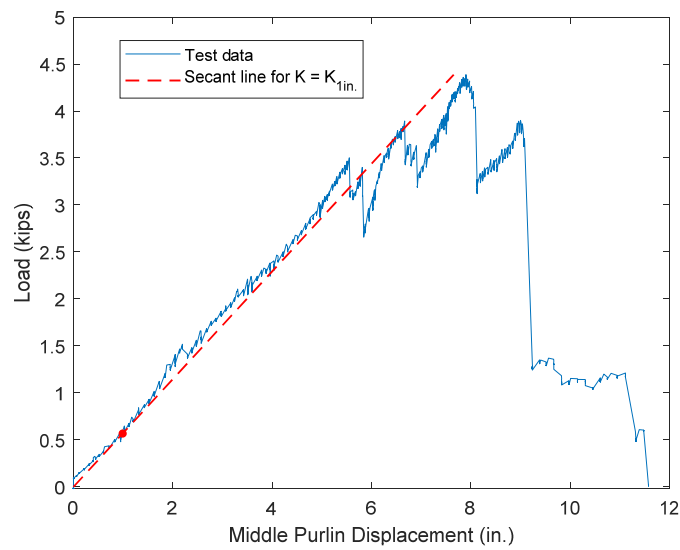


Figure A11-1 Load-displacement curve for Specimen 11

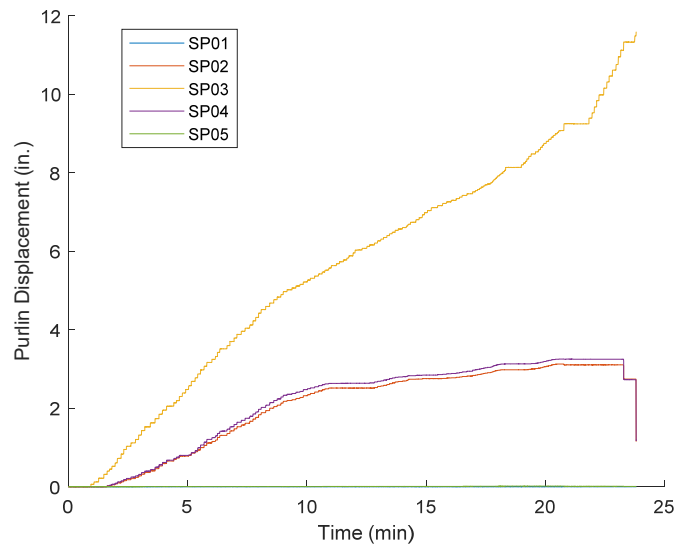


Figure A11-2 Purlin displacements of Specimen 11



Figure A11-3 Deformed shape of Specimen 11



Figure A11-4 Clip damage of Specimen 11